Mon. Not. R. Astron. Soc. **316**, 267–282 (2000)

Clustering of galaxies around radio quasars at $0.5 \leq z \leq 0.8$

Margrethe Wold,[1,2]★ Mark Lacy,[3] Per B. Lilje[2] and Stephen Serjeant[4]

[1]*Stockholm Observatory, SE-133 36 Saltsjöbaden, Sweden*
[2]*Institute of Theoretical Astrophysics, University of Oslo, PO Box 1029 Blindern, N-0315 Oslo, Norway*
[3]*Astrophysics, Nuclear and Astrophysics Laboratory, Keble Road, Oxford OX1 3RH*
[4]*Astrophysics Group, Imperial College London, Blackett Laboratory, Prince Consort Road, London SW7 2BZ*

Accepted 2000 February 22. Received 1999 October 11; in original form 1999 May 12

ABSTRACT

We have observed the galaxy environments around a sample of 21 radio-loud, steep-spectrum quasars at $0.5 \leq z \leq 0.82$, spanning several orders of magnitude in radio luminosity. The observations also include background control fields used to obtain the excess number of galaxies in each quasar field. The galaxy excess was quantified using the spatial galaxy–quasar correlation amplitude, $B_{\rm gq}$, and an Abell-type measurement, $N_{0.5}$. A few quasars are found in relatively rich clusters, but on average, they seem to prefer galaxy groups or clusters of approximately Abell class 0. We have combined our sample with literature samples extending down to $z \approx 0.2$ and covering the same range in radio luminosity. By using the Spearman statistic to disentangle redshift and luminosity dependences, we detect a weak, but significant, positive correlation between the richness of the quasar environment and the radio luminosity of the quasar. However, we do not find any epoch dependence in $B_{\rm gq}$, as has previously been reported for radio quasars and galaxies. We discuss the radio luminosity–cluster richness link and possible explanations for the weak correlation that is seen.

Key words: galaxies: active – galaxies: clusters: general – quasars: general.

1 INTRODUCTION

Since the discovery of quasars, much effort has been expended in trying to understand the physics of active galactic nuclei (AGN). Most work has concentrated on their nuclei, but during the last 10–15 yr the galaxy environments around different classes of AGN have received much attention.

The first studies that were made in this field (e.g. Stockton 1978; Longair & Seldner 1979; Yee & Green 1984, 1987, hereafter YG87; Prestage & Peacock 1988, 1989; Yates, Miller & Peacock 1989) showed that radio quasars and galaxies are located in regions of enhanced galaxy density. These findings were confirmed by more recent studies (e.g. Ellingson, Yee & Green 1991, hereafter EYG91; Hill & Lilly 1991; Allington-Smith et al. 1993; Fisher, Bahcall & Kirhakos 1996; Zirbel 1997), which added more weight to the consensus that the very local environment may be important for the formation and evolution of AGN. It is believed that AGN formation is closely related to the formation of supermassive black holes, possibly by galaxy–galaxy interactions and mergers. Interactions and mergers may also provide the fuel supply to a pre-existing central black hole. The study of AGN environments may therefore provide important clues about their formation and evolution.

★ E-mail: wold@astro.su.se

Radio-loud AGN are found to be associated almost exclusively with giant elliptical host galaxies (e.g. Taylor et al. 1996; Lacy et al. 1999 and references therein). Both the need for interaction, and the apparent need for a massive host, make it not surprising that groups or clusters of galaxies might be associated with radio-loud AGN. Furthermore, because the efficiency of conversion of the bulk kinetic energy of the radio jets to radio luminosity increases with environmental gas density, selection effects will also tend to favour finding steep-spectrum radio sources in gas-rich environments, i.e. in groups or clusters. High-z radio-loud AGN can therefore be used as tracers of groups and clusters at early epochs, and the evolution of galaxy groups and clusters can thus be studied independent of the selection biases associated with optical or X-ray cluster surveys.

Studying AGN environments may also help establish the relationship between different classes of AGN. In particular it has been proposed that radio galaxies and radio-loud quasars are the same type of object, but viewed at different orientations to the line of sight (Scheuer 1987; Barthel 1989; Antonucci 1993). The most robust test of such orientation-based 'unified models', is to select the AGN in question with one orientation-independent quantity (e.g. radio lobe luminosity) and compare another (e.g. environment). Indeed, observations of fields around radio-loud quasars and galaxies show that they are sited in environments that occupy approximately the same range in galaxy density (e.g.

Longair & Seldner 1979; Smith & Heckman 1990; Hill & Lilly 1991; Yee & Ellingson 1993).

For obvious reasons, most studies have been concerned with sources at $z \lesssim 0.6$, but recently various lines of evidence point to radio-loud AGN being in cluster environments also at $z \gtrsim 1$ (e.g. Dickinson 1994; Hall & Green 1998). Complications due to the possibility of lensing bias (Hammer & Le Fèvre 1990; Fort et al. 1996; Benítez, Martínez-González & Martín-Mirones 1997; Schneider et al. 1998), the possibility of non-thermal contributions to X-ray emission, and the low contrast of clusters against the background, however, make detections of clusters at these redshifts hard to prove.

An apparent decrease in the galaxy density around powerful (FR II) quasars from $z \sim 0.5$ to the present epoch has been observed (YG87; EYG91), although the amount of evolution is still not firmly established. Several investigators have also found that powerful FR II radio galaxies inhabit richer galaxy clusters at $z \sim 0.5$ than at $z \lesssim 0.3$. On the other hand, the less powerful FR I galaxies seem to be commonly found in clusters at both higher and lower redshifts (Longair & Seldner 1979; Prestage & Peacock 1988, 1989; Hill & Lilly 1991; Zirbel 1997). Yates et al. (1989) studied the environments of powerful radio galaxies in a wide redshift range and found that sources at $z > 0.3$ reside in clusters of typically Abell (1958) richness class 0, while the environments at $z < 0.3$ are three times poorer. Hill & Lilly (1991) compared a sample of radio galaxies at $z \approx 0.5$ spanning a wide range in radio luminosity with a lower redshift sample by Prestage & Peacock (1988, 1989) and confirmed the Yates et al. result. Allington-Smith et al. (1993) also arrived at a similar result, but with a less strong correlation between redshift and richness.

Most of the samples that have been studied are flux-limited, i.e. they suffer from a strong correlation between redshift and radio luminosity. This raises the possibility that the observed evolution in richness is dependent on radio luminosity rather than redshift. Yates et al. (1989) believed that this was the case in their study, but they were unable to confirm it since their sample had this strong redshift-radio luminosity correlation. However, for radio galaxies, Hill & Lilly (1991) were able to show that this is not the case by observing $z \sim 0.5$ sources over a wide range in radio luminosity. They found no correlation between richness and radio luminosity within their sample.

In this paper, we investigate the situation at $0.5 \leq z \leq 0.82$ for radio-loud quasars. This redshift range was chosen to extend previous work, which went up to $z \sim 0.6$, to as high a redshift as possible consistent with keeping the redshifted 4000-Å break shortward of the *I*-band. We selected quasars randomly from flux-limited samples spanning as wide a range in radio luminosity as possible. By extending the redshift range of previous studies, whilst maintaining the luminosity range, we are able to better disentangle trends in environmental richness due to cosmic evolution from those due to radio luminosity. The work presented here is also part of a larger study which aims at investigating and comparing the galaxy environments of different classes of AGN within a relatively small redshift range, but over as wide a luminosity range as possible.

We quantify the amount of galaxy clustering in each quasar field using the spatial quasar–galaxy cross-correlation amplitude, $B_{\rm gq}$, and an Abell-type measurement, $N_{0.5}$. These two quantities are briefly described in Section 2. In Sections 3 and 4, we present the quasar sample and describe the observations. The data reduction, photometry and faint-object detection in the charge-coupled device (CCD) images are discussed in Section 5. In Section 6, we quantify the galaxy environments in the quasar fields using $B_{\rm gq}$ and $N_{0.5}$, and compare our results with previous work on radio-loud AGN and other two-point correlation functions. In Section 7, we investigate redshift and luminosity dependences in $B_{\rm gq}$ in our own sample, and in a combined sample where our sources are put together with radio-loud quasars from other studies. We discuss our findings in Section 8, and the results are summarized in Section 9.

Unless otherwise specified, we have assumed an Einstein–deSitter universe model with $H_0 = 50\,{\rm km\,s^{-1}Mpc^{-1}}$ and $q_0 = 0.5$ throughout the analysis. Also, in this paper, 'quasar' should be interpreted as 'radio-loud quasar'.

2 QUANTIFYING GALAXY EXCESS

2.1 Galaxy–quasar cross-correlation amplitude

The use of the amplitude of the spatial cross-correlation function as a measure of galaxy excess was initiated by Seldner & Peebles (1978) and Longair & Seldner (1979). Since then, it has been widely used by other investigators for quantifying galaxy environments around various types of AGN at both lower and higher redshifts (e.g. Yee & Green 1984; YG87; Prestage & Peacock 1988, 1989; Yates et al. 1989; EYG91; Smith, O'Dea & Baum 1995; Wurtz et al. 1997; De Robertis, Yee & Hayhoe 1998). We only give the expressions here, but a detailed derivation may be found in Longair & Seldner (1979).

The spatial cross-correlation function, $\xi(r)$, is found to be well fit by a power law with slope γ and amplitude $B_{\rm gq}$,

$$\xi(r) = B_{\rm gq} r^{-\gamma},$$

where $B_{\rm gq}$ is the amplitude we seek in this analysis. In order to determine $B_{\rm gq}$ from the data, the amplitude, $A_{\rm gq}$, of the *angular* cross-correlation function, $\omega(\theta) = A_{\rm gq}\theta^{1-\gamma}$, must first be determined. An estimator for this amplitude is:

$$A_{\rm gq} = \frac{N_{\rm tot} - N_{\rm b}}{N_{\rm b}} \frac{3-\gamma}{2} \theta^{\gamma-1}, \qquad (1)$$

which is directly obtainable from galaxy counts in the quasar fields and in images of background control fields. In the above expression, $N_{\rm tot}$ is the number of galaxies in the quasar field within a circle of radius θ centred on the quasar, corresponding to 0.5 Mpc at the quasar redshift. The number of background galaxies from the control fields is denoted by $N_{\rm b}$. The slope of the correlation function, γ, is usually assumed to be 1.77, as found by Groth & Peebles (1977) for the low-redshift galaxy–galaxy correlation function. YG87 showed that the galaxy–quasar correlation function has a slope consistent with this. Lilje & Efstathiou (1988), however, found $\gamma = 2.2$ in a study of the cross-correlation between Abell clusters and the Lick galaxy counts down to scales of 0.2 Mpc, but Prestage & Peacock (1988, 1989) have demonstrated that $B_{\rm gq}$ is insensitive to an incorrect choice of γ, provided that $\gamma \sim 2$. We have therefore made the usual assumption that $\gamma = 1.77$.

The spatial correlation amplitude is obtained from $A_{\rm gq}$ by the relation:

$$B_{\rm gq} = \frac{\mathcal{N}_{\rm g} A_{\rm gq}}{\Phi(m_{\rm lim}, z) I_\gamma} d_\theta^{\gamma-3},$$

where $\mathcal{N}_{\rm g}$ is the average surface density of background galaxies and d_θ is the angular diameter distance to the quasar. The two quantities in the denominator are $I_\gamma = 3.78$, which is an

integration constant, and $\Phi(m_{\rm lim}, z)$, which denotes a universal luminosity function integrated down to the apparent completeness limit at the quasar redshift: $\Phi(m_{\rm lim}, z) = \int_{L(m_{\rm lim},z)}^{\infty} \phi(L)\,{\rm d}L$. The integrated luminosity function gives the number of field galaxies per unit volume at the quasar redshift with magnitudes brighter than the completeness limit of the data. By normalizing $B_{\rm gq}$ with $\Phi(m_{\rm lim}, z)$, an absolute measure of the galaxy excess at the quasar redshift is obtained, but unfortunately the luminosity function is poorly constrained at higher redshifts. This a critical step in the analysis, especially since $B_{\rm gq}$ is inversely proportional to the normalization, ϕ^*, of this luminosity function. As advocated by YG87 and Yee & López-Cruz (1999), it is therefore important that ϕ^* is consistent with the background galaxy counts obtained from the data. In our analysis, we have used the Canada–France Redshift Survey (CFRS) luminosity function (Lilly et al. 1995) to track the evolution of the characteristic luminosity L^*, and then used the observed galaxy counts in order to fit ϕ^* as a function of redshift. This is described in more detail in Section 6.

2.2 A more direct measurement

The quantity $N_{0.5}$, first introduced by Hill & Lilly (1991), provides a more direct, but less deep measure of the clustering strength than $B_{\rm gq}$. The galaxy counting is restricted to a certain magnitude interval, but a separate calculation of the luminosity function is not required. Hill & Lilly used it for quantifying galaxy environments around a sample of radio galaxies. For a radio galaxy with apparent magnitude $m_{\rm g}$, $N_{0.5}$ is the number of excess galaxies with magnitudes in the range $m_{\rm g}$ to $m_{\rm g} + 3$ within a radius of 0.5 Mpc centred on the radio galaxy. Since the quasar appears as a bright stellar object, the magnitude of the host galaxy cannot be directly determined. Instead, we have estimated $m_{\rm g}$ for the quasar host from the magnitude–redshift relation for radio galaxies of Eales (1985):

$$m_{\rm g}(R) = 21.05 + 5.3 \log z, \qquad (2)$$

valid for $19.0 < m_{\rm g}(R) < 21.3$. Some of our quasar fields were also imaged in I, and in this case we estimated $m_{\rm g}(I)$ by subtracting the $R - I$ colour of an E/S0 galaxy model (Guiderdoni & Rocca-Volmerange 1988) from $m_{\rm g}(R)$. The $N_{0.5}$ measurement may suffer from systematic errors with redshift if radio galaxies and clusters galaxies evolve differently in luminosity. At these redshifts, however, the effect is likely to be small, and we have therefore not taken it into account.

3 SAMPLE SELECTION

The sample investigated here consists of 21 radio-loud steep-spectrum ($\alpha > 0.5$ where radio flux density is $S_\nu \propto \nu^{-\alpha}$) quasars with redshifts $0.5 \le z \le 0.82$ covering the radio luminosity range $23.8 \le \log(L_{408\,\rm MHz}/{\rm WHz^{-1}\,sr^{-1}}) \le 26.7$. The sources were divided into high- and low-radio luminosity sub-samples selected from two different radio/optical flux-limited samples in order to better distinguish between luminosity and redshift dependences.

The eleven sources in the low-luminosity sample were drawn from the 7C quasar (7CQ) survey (Riley et al. 1999) which consists of 7C sources with a flux density limit of $S_{151\,\rm MHz} > 0.1$ Jy (≈0.05 Jy at 408 MHz) identified with objects on POSS–I (Palomar Observatory Sky Survey) E-plates with $E < 20$ and colour $O - E < 1.8$ ($E \simeq R$ and $O \simeq B$). Consequently, the 7CQ survey finds only the optically brightest steep-spectrum quasars at any redshift. Willott et al. (1998) estimate the 7CQ survey to be 40 per cent complete due to the bright optical magnitude limit. However, at $z = 0.5$ and $z = 0.8$, the optical flux limit corresponds to $M_B = -21.7$ and $M_B = -22.7$ respectively (for K-corrections, see below), hence according to the definition employed by Willott et al., where a quasar must have $M_B < -23$, the 7CQ sample is complete in our redshift range. Clearly though, this is a rather artificial distinction, and we will be missing many broad-line objects with fainter nuclei.

The eight sources in the high-luminosity sample were drawn from the Molonglo/APM Quasar Survey (MAQS) (Serjeant 1996; Maddox et al., in preparation; Serjeant et al., in preparation) which consists of sources with radio flux densities $S_{408\,\rm MHz} \ge 0.95$ Jy from the Molonglo Reference Catalogue (MRC) (Large et al. 1981) identified with objects on the UK Schmidt plates having $b_{\rm J} < 22.5$. The MAQS thus have a faint optical completeness limit and a relatively bright radio flux density limit, and its completeness was estimated to be 99 per cent by Willott et al. (1998).

We also included two more quasars in the sample, 3C 380 and 5C 6.189. The most powerful source, 3C 380, was selected from the 3CRR sample of Laing, Riley & Longair (1983), which has a flux limit of $S_{178\,\rm MHz} > 10.9$ Jy (≈6.05 Jy at 408 MHz). The radio quasar 5C 6.189 was selected from the $0.1 < S_{151\,\rm MHz} < 0.5$ Jy complete sample of Rossitter (1987), which has essentially the same selection criteria as the 7C sources, so 5C 6.189 is included in the low-luminosity sample. This quasar has a spectral index of 0.36, so strictly speaking it does not belong with the other steep-spectrum sources in the sample. It is unresolved to a limit of 3 arcsec in radio images, and since it also has a low radio luminosity we believe that it might be the Doppler boosted core of an intrinsically much less luminous radio source. We therefore neglected this object in the correlation analysis in Section 7.

The majority of the sources in the sample exhibit FR II morphology with bright cores, jets, edge-brightened lobes and hotspots, typical of radio-loud quasars. Two of the 7C and four of the MRC quasars are compact steep-spectrum (CSS) sources. CSS sources have apparent sub-galactic sizes (<30 kpc) in radio and are thought to be intrinsically compact rather than being extended sources shortened by projection effects (Fanti et al. 1990). It is believed that the CSS sources are either young radio sources in the stage of formation, or that they are confined by a high-density ISM in the host galaxy which is likely to be denser than the IGM/ICM confining the more extended radio sources. It is uncertain whether this will bias the CSS sources in the sample toward richer or

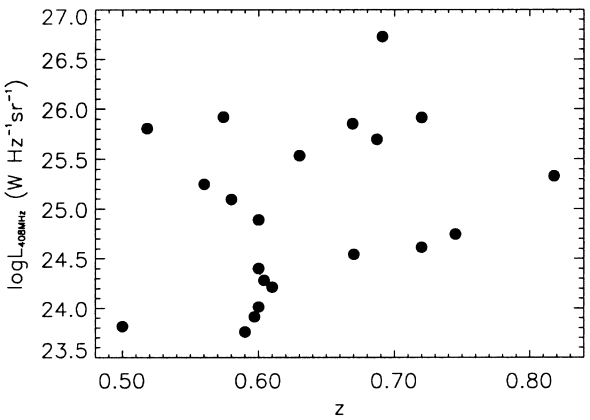

Figure 1. Radio luminosity at 408 MHz of quasars in the sample as a function of redshift. The luminosities were calculated from flux densities and spectral indices given in Table 1.

Table 1. Basic data of the sources in the radio-loud quasar sample. The spectral index, α, is defined in the sense that radio flux density is $S_\nu \propto \nu^{-\alpha}$. The data on the MRC and 7C quasars are from Serjeant (1996) and Riley et al. (1999), respectively. Redshift and flux density of 5C 6.189 are from Rossitter (1987) and the redshift of 3C 380 from Laing et al. (1983). The flux densities at 408 MHz of the 7C quasars were calculated from flux densities at 151 MHz, assuming spectral indices as given in the table.

Source	z	M_B	S_{408} (Jy)	α	Radio size (kpc)	Radio morphology[a]
MRC 0032−203	0.518	−21.48	6.870	1.10	21.7	CSS (borderline)
MRC 0033−000	0.560	−22.44	1.790	0.86	29.4	CSS (borderline)
MRC 0106−233	0.818	−23.96	1.130	0.60	20.7	CSS (borderline)
MRC 0144−058	0.630	−23.30	2.880	0.72	52.6	FR II
MRC 0159−117	0.669	−24.88	5.700	0.58	118.4	FR II
5C 6.189	0.597	−23.93	0.091	0.36	<22.9	compact
MRC 0222−008	0.687	−23.28	3.150	0.92	106.5	FR II
MRC 0405−123	0.574	−24.86	8.170	0.80	260	FR II
MRC 0406−180	0.720	−22.29	5.600	0.60	<4	CSS
7C 2671	0.745	−22.97	0.340	0.68	341.0	FR II
7C 2676	0.604	−25.80	0.202	0.43	191.2	FR II
7C 2704	0.580	−23.04	1.232	0.74	4.5	CSS
7C 2867	0.600	−23.86	0.230	0.76	381.5	FR II
7C 2886	0.610	−23.52	0.148	0.71	76.7	FR II
7C 2928	0.720	−24.05	0.256	0.77	314.0	FR II
7C 3066	0.600	−24.52	0.671	0.88	312.9	FR II
7C 3201	0.500	−24.23	0.085	0.81	300.0	FR II
7C 3222	0.670	−24.34	0.270	0.64	347.4	FR II
7C 3450	0.590	−23.41	0.056	0.69	7.6	CSS
7C 3814	0.600	−24.81	0.094	0.76	137.4	FR II
3C 380	0.691	−25.81	37.78	0.69	27.1[b]	FR II

[a] The radio sizes and morphologies were determined from maps by Kapahi et al. (1998) (MRC 0032−203 and 0106−233), Morganti, Killeen & Tadhunter (1993) (MRC 0159−117 and 0405−123), Rossitter (1987) (5C 6.189), Downes et al. (1986) (MRC 0222−008), Reid et al. (1995) (3C 380) and Riley et al. (1999) (7C sources). An *L*-band VLA map of MRC 0406−180 is presented in Best, Röttgering & Lehnert (1999) where it is consistent with being unresolved, and it is used as a VLA phase calibrator at *L*-band in A-array, so must have an angular size $\lesssim$0.5 arcsec. Radio sizes for MRC 0033−000 and 0144−058 are from Blundell (private communication).
[b] 3C 380 appears compact, but its intrinsic size is probably larger than 30 kpc since there is evidence for superluminal motion in this source (Wilkinson et al. 1990).

poorer galaxy environments, since it is difficult to see a reason for a correlation between the local gas density in the core of the host galaxy and the gas density (or the galaxy density) on Mpc scale in the surrounding cluster.

In Fig. 1 we have plotted the radio luminosity of the quasars in the sample as a function of redshift, and various properties of the sources are listed in Table 1. The quasar B luminosities in this table were calculated as follows: For the MRC quasars, we obtained m_B from APM magnitudes assuming $m_{\rm APM} \approx 29.42 - b_{\rm J}$ (Maddox, personal communication) and $b_{\rm J} \approx m_B - 0.09$ (Metcalfe et al. 1991). For the 7C sources, we calculated m_B from E mag by first assuming $R \approx E$ and thereafter converting to B by assuming a power-law spectrum $S_\nu \propto \nu^{-0.5}$ and using the B and R zero points given by Longair (1981). The m_B mag of 5C 6.189 and 3C 380 were found from R and B mag given by Rossitter (1987) and Netzer et al. (1996), respectively. The apparent magnitudes were thereafter converted to absolute M_B luminosities by assuming a K-correction equal to $2.5(\alpha - 1)\log(1 + z)$.

All sources, except 3C 380 and 5C 6.189, have galactic latitudes $|b| > 42°$ and galactic reddening $E(B - V) < 0.04$. 3C 380 and 5C 6.189 lie at latitudes 23°.5 and 27°.3 and have galactic reddening of 0.07 and 0.06, respectively.

4 OBSERVATIONS

Most of the quasar fields were imaged with the HiRAC camera at the 2.56-m Nordic Optical Telescope (NOT) at La Palma, Spain, during 1994 December 23–25 and 1997 May 10–15. The 7C 3222 and 7C 3450 fields were imaged with the 107-inch telescope at the McDonald Observatory in Texas during 1996 February 17–22. Images were also taken of several background control fields to provide a measurement of the field galaxy counts. The least biased way of obtaining background galaxy counts is to estimate it from the edges of the quasar fields, but the HiRAC CCD at the NOT has too small a field of view (3×3 arcmin^2) for this approach. The background images were therefore obtained by offsetting the telescope 5 or 10 arcmin either north or south of sources in our AGN sample, or by selecting a random position in the sky at a similar galactic latitude as the programme targets.

To extend our low radio luminosity sample, we used data on five 7C quasars obtained with the *Hubble Space Telescope* (Serjeant, Rawlings & Lacy 1997; Serjeant et al. 2000, in preparation). These images were taken in the F675W-filter in 4×500 s exposures with the WFPC2. In Table 2, positions and details about the observations of the quasar and background fields are provided.

Eight of the quasar fields were imaged in two filters, either V and R, or R and I, depending on the redshift of the quasar, in order to straddle the 4000-Å break in the quasar rest frame. This was done with the aim of using colours to study the evolution of the cluster galaxies, and to isolate cluster members with strong 4000-Å breaks. These studies will be discussed in a future paper. Quasars with redshifts $z < 0.67$ were imaged in V and R, whereas quasars with $z \geq 0.67$ were imaged in R and I. For the fields that

Table 2. Positions and details about the observations of the quasar (upper part) and background fields (lower part). 'NOT' is the Nordic Optical Telescope, 'McD' is the 107-inch telescope at the McDonald Observatory and '*HST*' is the *Hubble Space Telescope*.

Source	RA (1950)	DEC (1950)	Filter	Exp. time (s)	Telesc., date
MRC 0032−203	00:32:38.61	−20:20:29.58	*R*	4 × 600	NOT 94Dec23
MRC 0033−000	00:33:53.28	−00:03:27.35	*R*	4 × 600	NOT 94Dec25
MRC 0106−233	01:06:37.57	−23:23:27.63	*R*, *I*	4 × 600	NOT 94Dec23,24
MRC 0144−058	01:44:14.29	−05:52:56.58	*R*	4 × 600	NOT 94Dec 24
MRC 0159−117	01:59:30.39	−11:47:00.12	*R*	4 × 600	NOT 94Dec 24
5C 6.189	02:15:45.30	+31:35:39.60	*R*	4 × 600	NOT 94Dec 25
			R	1 × 300[a]	NOT 96July21
MRC 0222−008	02:22:34.59	−00:49:03.89	*R*, *I*	4 × 600	NOT 94Dec23
MRC 0405−123	04:05:27.50	−12:19:32.52	*V*, *R*	4 × 600	NOT 94Dec23,24
MRC 0406−180	04:06:52.14	−18:05:02.39	*R*, *I*	4 × 600	NOT 94Dec24
7C 2671	10:19:33.03	+45:56:16.10	*R*, *I*	4 × 600	NOT 97May11,10
7C 2676	10:19:42.68	+39:46:42.99	F675W	4 × 500	*HST* 95Oct16
7C 2704	10:20:08.78	+48:07:10.41	F675W	4 × 500	*HST* 96Jan12
7C 2867	10:24:04.46	+41:54:38.75	F675W	4 × 500	*HST* 95Nov15
7C 2886	10:24:28.39	+43:06:59.89	F675W	4 × 500	*HST* 95Oct15
7C 2928	10:25:34.68	+43:21:46.30	*I*	9 × 300	NOT 97May14
7C 3066	10:28:47.86	+42:09:46.30	*V*, *R*	4 × 600	NOT 94Dec24
7C 3201	10:32:10.50	+39:26:01.66	F675W	4 × 500	*HST* 95Nov6
7C 3222	10:32:21.15	+34:21:58.10	*R*, *I*	11 × 300	McD 96Feb20
7C 3450	10:37:26.01	+45:05:14.10	*R*	11 × 300	McD 96Feb21
7C 3814	10:45:16.82	+38:53:27.60	*V*, *R*	4 × 600	NOT 94Dec23
3C 380	18:28:13.55	+48:42:40.38	*I*	8 × 300	NOT 97May13,14
0332−1152	03:32:45.60	−11:52:07.10	*I*	5 × 600	NOT 94Dec23
0405−1209	04:05:27.43	−12:09:29.10	*R*	4 × 600	NOT 94Dec24
1018+4556	10:18:58.00	+45:56:22.80	*I*	9 × 300	NOT 97May11,13
1025+4311	10:25:34.43	+43:11:49.00	*I*	9 × 300	NOT 97May14
1032+3416	10:32:21.15	+34:16:58.10	*R*, *I*	11 × 300	McD 96Feb20
1037+4510	10:37:26.01	+45:10:14.10	*R*	6 × 300	McD 96Feb21
1217+3650	12:17:40.13	+36:50:45.50	*I*	11 × 300	McD 96Feb18
1349+6434	13:49:13.18	+64:34:24.00	*I*	4 × 600	NOT 97May10
1545+4745	15:45:00.00	+47:45:00.00	*R*, *I*	4 × 600	NOT 96July21
1755+6820	17:55:55.07	+68:20:54.10	*R*, *I*	4 × 600	NOT 97May11,13,10
1758+6500	17:58:00.00	+65:00:00.00	*I*	4 × 600	NOT 96July24
1807+6821	18:07:00.05	+68:21:11.50	*R*	4 × 600	NOT 97May14
2235+0130	22:35:00.00	+01:30:00.00	*V*, *R*	4 × 600	NOT 96July21
2238+0200	22:38:00.00	+02:00:00.00	*R*, *I*	4 × 600	NOT 96July22,23
2355+0240	23:55:00.00	+02:40:00.00	*V*, *R*	4 × 600	NOT 96July24

[a]Short exposure to enable deeper non-photometric images of this field to be properly calibrated.

Table 3. The observing runs.

Date	Telesc.	CCD	FOV (arcmin^2)	Pixel scale (arcsec pixel^{-1})	Average seeing (arcsec)	Extinction in *V* (mag)	Remarks
1994 Dec 23,24[a]	NOT	1k SiTe	3 × 3	0.176	0.6	0.13	photometric
1994 Dec 25	NOT	1k SiTe	3 × 3	0.176	1.0	0.13	variable transparency
1996 Feb 17–22	McD	1k TEK	11 × 11	0.700	2–3	0.17	partly cloudy
1996 July 21–23	NOT	1k SiTe	3 × 3	0.176	0.7	0.1–0.2	photometric
1996 July 24	NOT	1k SiTe	3 × 3	0.176	0.7	0.34	dust in the air
1997 May 10[b]–14	NOT	2k Loral	3.7 × 3.7	0.110	0.7–0.8	0.13	some nights clear, some with cirrus

[a] Most of the radio-loud quasar fields were obtained during December 23–24.
[b] On May 10 the CCD had lost its quantum efficiency in blue resulting in a 0.5-mag reduction in the *I*-band sensitivity.

were imaged in only one filter, *R* was chosen for $z < 0.67$ and *I* for $z \geq 0.67$. Six of the background fields were also imaged in two filters. With a few exceptions, the exposure time in every quasar and background field is 4 × 600 s (or 9 × 300 s), so that all fields have a similar depth. The images from the 107-inch telescope have exposure times of 11 × 300 s since the CCD was less sensitive than the CCD at the NOT, and the seeing was poorer. The weather and seeing conditions during the observations, as well as details about the CCDs that were used, are given in Table 3. For standard star calibration, we observed fields from Christian et al. (1985) during all observing runs.

5 DATA REDUCTION AND PHOTOMETRY

The preprocessing of the images was performed with IRAF. Twilight flats were used to flat-field the NOT data, but the *I*-band data from the 1997 May run were also flat-fielded with a skyflat formed by medianing 9–10 frames in order to remove fringing.

After co-aligning the images, they were averaged together and cosmic rays were removed.

The McDonald data were corrected for dark current and flat-fielded with either twilight or dome flats. Since these data suffer from a partially cloudy sky, some extra reduction steps were found necessary. All images were divided with a skyflat in order to remove flat-field variations during the night, and to improve the removal of the vignetting at the edge of the field. To take out the effect of clouds, some of the images were scaled so that some reference star in each image had the same flux as measured in the best image. Each scaled frame was then multiplied with a weight factor inversely proportional to the variance before co-aligning and combining.

The *HST* (*Hubble Space Telescope*) data were corrected for bad pixels using the bad pixel maps, and thereafter combined using the IRAF/STSDAS task CRREJ in order to remove cosmic rays.

5.1 Photometry and object detection

For object detection and photometry of faint galaxies in the CCD images we utilized FOCAS (Faint Object Classification and Analysis System, e.g. Valdes 1989). The detection limit in FOCAS was set to 2.5σ above sky level and the 'built-in' detection filter was used, a 5×5 pixel array designed to increase the sensitivity to extended objects with low surface brightness. Furthermore, objects were detected only if they had sizes larger than a minimum size which was determined for each frame by measuring the average seeing from stars in the image. Objects were therefore recognized only if they had N contiguous pixels above the sky level, where N was varied to match the seeing and the pixel scale of the CCD. To estimate the magnitudes of the detected objects we used FOCAS total magnitudes. The total magnitudes in FOCAS are evaluated by filling in concavities in the isophote shapes until the area is twice the isophotal area and then measuring the flux above sky level within this expanded region. The FOCAS total magnitudes have been shown to give good estimates of true magnitudes (Koo, Ellis & Windhorst 1989).

No attempt was made to separate stars and galaxies in the images, because the wide range in seeing conditions in which the data were taken made it hard to perform such separation reliably. Since the background fields were taken at similar galactic latitudes as the quasar fields, the number of stars is approximately the same in both. Stars will therefore statistically be accounted for in the analysis. Also, at high galactic latitudes, galaxies are expected to dominate the counts fainter than $R \sim 20$. Each detected object was classified by FOCAS by using a template point spread function, which was formed from typically 4–5 selected stars in each image. When we counted the number of objects in the images, we excluded objects that were classified as 'n' (noise) or 'long', and also in a few cases, objects coinciding with the spikes of bright stars.

Magnitudes measured in the F675W filter were calibrated to Johnson R by using photometry of objects in fields that were imaged both with the *HST* and the NOT. With this approach, we found a zero point of 21.78 ± 0.47 mag, which is similar to the one obtained by using the *photflam* and *photzpt* header keywords to compute a magnitude in the STMAG system, and then convert to Johnson R as described in the WFPC2 Instrument Handbook (Biretta et al. 1996).

All magnitudes were corrected for galactic extinction using the maps of Burstein & Heiles (1982) and the Galactic extinction law by Cardelli, Clayton & Mathis (1989).

5.2 Completeness simulations

To find the completeness limit and to gain as much information at faint magnitudes as possible, we simulated the loss of galaxies (in the ground-based data) in both the quasar and the background images due to incompleteness. We utilized ARTDATA in IRAF to add a grid of ~70 artificial galaxies with known magnitudes (typically 20–25 mag) and half-light radii distribution according to the *HST* Medium Deep Survey (Schmidtke et al. 1997). Two different galaxy profiles were chosen in order to investigate which galaxies were most easily picked up by FOCAS, exponential discs resembling spiral galaxies and de Vaucouleurs profiles resembling elliptical galaxies. Inclination and position angles were randomly distributed.

After adding the artificial galaxies, the CCD frames were processed in FOCAS and the result of the detection process examined to find how many of the added galaxies were detected, and what their total magnitudes had been estimated to. This process was repeated several times, each time turning the flux of the galaxies down by 0.1 mag, until the fraction picked up by FOCAS had decreased significantly.

By comparing the FOCAS-computed total magnitudes with the magnitudes originally assigned to the galaxies, we were able to estimate the errors made by FOCAS as a function of magnitude. These simulations show that the NOT data are complete down to 23.5 in R and 23.0 mag in I with errors of ± 0.3 mag at the faintest limit. The data from the 107-inch telescope are less deep with a completeness limit of 22.5 in R and 21.5 mag in I with errors of ± 0.4 mag at the limit. Furthermore, galaxies with exponential disc profiles were more easily detected than those with de Vaucouleurs profiles.

In intervals of half a magnitude, we calculated the fraction of galaxies detected in FOCAS by averaging the detected fractions of exponential and de Vaucouleurs profiles. In order to correct for incompleteness at faint magnitudes, the number of galaxies in every magnitude bin was divided by the detected fraction in the corresponding bin, but only as long as the correction was less than a factor of 2. The corrected counts were used to find deeper and incompleteness-corrected values of the correlation amplitudes. The WFPC2 images are deeper than the ground-based images in the sense that fainter galaxies will be more easily detected. However, since we only have ground-based background frames to normalize the counts, we took the same magnitude cut-off in the *HST* images as in the NOT images when computing $A_{\rm gq}$ and $B_{\rm gq}$.

6 RESULTS

6.1 Field galaxy counts

The background control images obtained at the NOT yield an area of 18 arcmin^2 in V, 58.7 arcmin^2 in R and 73.7 arcmin^2 in I, most of them taken during the observations in 1996 July and 1997 May. The background images from the 107-inch telescope cover an area of 103.3 and 97.7 arcmin^2 in R and I, respectively. Figs 2 and 3 show the number counts per deg^2 of field galaxies as obtained from the NOT images. The average number counts of galaxies in the quasar fields are also plotted. The number counts in these two figures have been corrected for incompleteness as described in Section 5.2, and the corrected field counts have slopes of 0.29 ± 0.05 and 0.34 ± 0.06 in R and I, respectively. In the R-band, the slope of the raw number counts is 0.24 ± 0.03, whereas for the raw I counts, the slope is 0.26 ± 0.06. Our estimates of the slopes

are in agreement with that found by others (Lilly, Cowie & Gardner 1991; Steidel & Hamilton 1993; Smail et al. 1995). For example, Smail et al. find a slope of 0.321 ± 0.001 in R and 0.271 ± 0.009 in I, which is within the errors of the slopes of our completeness corrected counts.

The error bars in Figs 2 and 3 were calculated as Poisson errors multiplied with a factor (1.3) that approximates the departure from Poisson statistics if there is a non-random distribution of field galaxies (Yee & López-Cruz 1999).

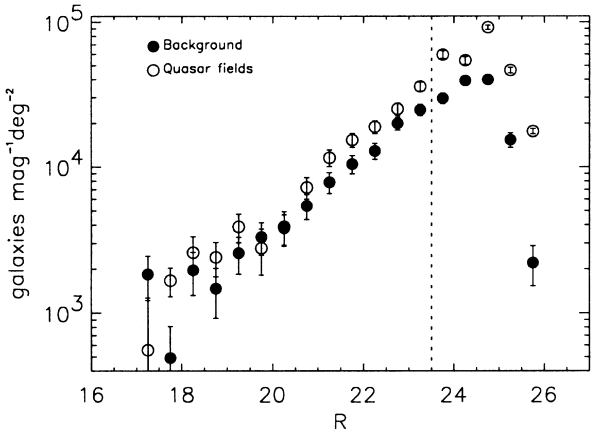

Figure 2. This plot compares the average number count of galaxies in the quasar (open circles) and the background images (filled circles). A clear excess of galaxies in the quasar fields is seen from $R \approx 20$. The completeness limit is indicated by the vertical dotted line. The slope of the background counts at $R > 20$ (where the counts are not contaminated by stars) was found to be 0.29 ± 0.05.

6.2 Calculation of A_{gq} and B_{gq}

In the quasar fields, we counted galaxies with magnitudes brighter than the completeness limit within a circle of 0.5 Mpc centred on the quasar (0.5 Mpc at $z = 0.7$ corresponds to ≈66 arcsec). The average background galaxy count down to the same magnitude was thereafter subtracted in order to give the excess number of galaxies, $N_{tot} - N_b$. Typical values of N_{tot} in the richest fields were 70–80 whereas the poorest fields had $N_{tot} \approx 20$–30. The background count, N_b, was typically around 45. A corrected excess was also calculated using the incompleteness corrected counts. In most fields this could be done down to a fainter

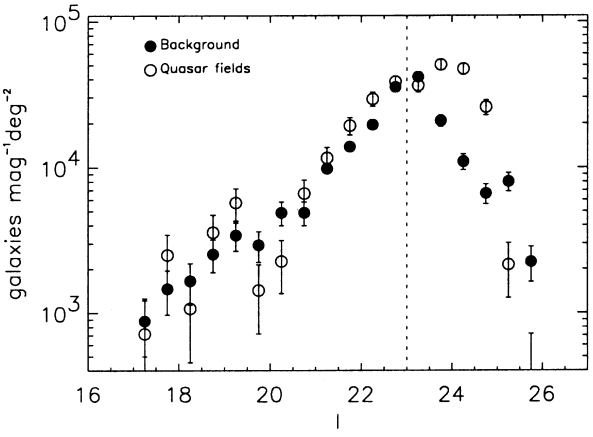

Figure 3. Same as in Fig. 2, but for counts in the I-band. The slope of the background counts at $I > 20$ is 0.34 ± 0.06. The 'bump' at $I < 20$ is probably caused by stars.

Table 4. Clustering statistics for the quasar fields consisting of the angular and the spatial galaxy–quasar cross-correlation amplitudes, A_{gq} and B_{gq}, and the more direct Abell-type measurement, $N_{0.5}$. The correlation amplitudes were calculated both from raw galaxy counts and from galaxy counts corrected for incompleteness. The magnitude limits were set to $R = 23.5$ and $I = 23.0$ for the raw counts, whereas a deeper limit was applied for the corrected counts, maximum 24.5 in R and 23.5 in I. The fields that are denoted 'unchanged' are fields that could not be pushed above the completeness limits of 23.5 in R and 23.0 mag in I. The corrected counts were not applied to the *HST* images either, as denoted by '…'. The errors in A_{gq} and B_{gq} are ΔA_{gq} and ΔB_{gq} from equation (3).

Source	z	$A_{gq} \times 10^{-3}$ (rad$^{0.77}$)	$A_{gq} \times 10^{-3}$ (corrected)	B_{gq} (Mpc$^{1.77}$)	B_{gq} (corrected)	$N_{0.5}$
MRC 0032−203	0.518	0.52 ± 0.26	0.48 ± 0.20	253 ± 127	303 ± 129	6.0 ± 8.2
MRC 0033−000	0.560	−0.24 ± 0.22	−0.13 ± 0.18	−142 ± 133	−100 ± 134	−3.5 ± 7.8
MRC 0106−233	0.818	0.00 ± 0.25	0.30 ± 0.21	−3 ± 233	345 ± 236	−3.8 ± 7.7
MRC 0144−058	0.630	0.62 ± 0.27	0.66 ± 0.19	421 ± 184	539 ± 157	25.0 ± 9.7
MRC 0159−117	0.669	0.31 ± 0.26	0.54 ± 0.19	272 ± 222	507 ± 177	5.6 ± 8.7
5C 6.189	0.597	1.07 ± 0.29	0.75 ± 0.22	685 ± 186	590 ± 170	15.4 ± 9.0
MRC 0222−008	0.687	0.36 ± 0.27	0.58 ± 0.22	246 ± 185	537 ± 197	2.0 ± 7.6
MRC 0405−123	0.574	0.94 ± 0.28	1.15 ± 0.23	579 ± 179	875 ± 176	12.7 ± 8.8
MRC 0406−180	0.720	0.79 ± 0.29	0.50 ± 0.21	569 ± 174	469 ± 201	−0.6 ± 7.6
7C 2671	0.745	0.04 ± 0.25	unchanged	35 ± 212	unchanged	−1.9 ± 7.5
7C 2676	0.604	−0.41 ± 0.21	…	−265 ± 138	…	−7.3 ± 6.8
7C 2704	0.580	0.41 ± 0.26	…	253 ± 160	…	11.6 ± 8.0
7C 2867	0.600	−0.04 ± 0.23	…	−25 ± 152	…	−0.2 ± 7.3
7C 2886	0.610	0.11 ± 0.24	…	70 ± 159	…	3.4 ± 7.6
7C 2928	0.720	−0.13 ± 0.24	unchanged	−94 ± 175	unchanged	−2.6 ± 7.4
7C 3066	0.600	0.22 ± 0.25	−0.21 ± 0.16	144 ± 161	−168 ± 126	0.4 ± 8.1
7C 3201	0.500	−0.06 ± 0.23	…	−29 ± 109	…	5.6 ± 7.6
7C 3222	0.670	−0.05 ± 0.38	0.03 ± 0.33	−52 ± 364	27 ± 259	−0.1 ± 5.7[a]
7C 3450	0.590	1.33 ± 0.44	1.49 ± 0.38	910 ± 297	895 ± 227	26.4 ± 7.7[b]
7C 3814	0.600	0.28 ± 0.25	0.44 ± 0.21	178 ± 163	350 ± 162	17.4 ± 9.1
3C 380	0.691	0.66 ± 0.28	unchanged	458 ± 198	unchanged	7.0 ± 7.9

[a] Counted within m_g and $m_g + 2.27$
[b] Counted within m_g and $m_g + 2.66$

magnitude than what we defined to be the completeness limit, but not fainter than 24.5 in R and 23.5 mag in I, since here the correction factor was greater than 2.

In order to prevent systematic errors, the quasar and background frames were treated identically during data reduction and object detection. Also, the background galaxy counts obtained at one of the two (NOT and 107 inch) different telescopes were applied only to quasar frames from the same telescope. The galaxy excess in the *HST* images was found by subtracting the NOT background counts. For fields that were imaged in two filters, we used the galaxy counts in the image taken through the reddest filter for computing $B_{\rm gq}$, since this gives preference to red galaxies that are likely to lie at the quasar redshift.

The field size of 3×3 arcmin^2 at the NOT was sufficient to cover the 0.5-Mpc radius, provided the quasar was well centred on the frame. Two of the quasar frames were nevertheless found to have parts of the circle lying outside the edges of the field. No large areas were missing, 0.28 arcmin^2 at the most, which is less than 8 per cent of the area of the circle. We also took out $\approx$6.5 per cent of the area in the MRC 0222−008 field because of a large, bright foreground galaxy. The missed and the chopped-out areas were corrected for by assuming a density of galaxies equal to the mean density within the remaining area. The same approach was applied to the *HST* data, where the 'L'-shaped field of view of the WFPC2 covered approximately half the area that we were interested in.

The excess number of galaxies in each field was used to find the angular cross-correlation amplitude, $A_{\rm gq}$. Computed values of $A_{\rm gq}$, both from the raw counts and from the corrected counts, are shown in Table 4. We also averaged together the galaxy number counts within the 0.5-Mpc radius in all the quasar fields and plotted it together with the field galaxy counts as shown in Figs 2 and 3 to demonstrate that there is a real excess of galaxies.

In order to obtain the spatial cross-correlation amplitude, $B_{\rm gq}$, the angular correlation amplitude has to be normalized with the number of field galaxies at the quasar redshift, as given by the integrated luminosity function, $\Phi(m_{\rm lim}, z)$. We used the Schechter (1976) function with parameters $\alpha = -0.89$ and $M^*_{AB}(B) = -20.83$ based on Lilly et al.'s (1995) estimation of the CFRS luminosity function at redshifts $0.5 \leq z \leq 0.75$. The values of ϕ^* employed were 0.0072 and 0.0052 Mpc^{-3} in R and I, respectively. Below, we explain how the ϕ^*'s were chosen in order to be consistent with the observed field galaxy counts. The CFRS luminosity function is well suited to our analysis, especially since CFRS is an I-band selected survey, and results from Lin et al. (1999) based on the CNOC2 (Canadian Network for Observational Cosmology) Field Galaxy Redshift Survey show that there is general agreement between the CFRS and the CNOC2 luminosity function.

To make sure that the observed background galaxy counts were consistent with the ϕ^* normalization, we constructed galaxy counts from a combination of four Schechter function segments. These constructed counts were compared to the observed counts to find the ϕ^* that best matched the data. We selected luminosity-function segments for four redshift intervals, $\langle 0.0, 0.2\rangle$, $\langle 0.2, 0.5\rangle$, $\langle 0.5, 0.75\rangle$ and $\langle 0.75, 1.0\rangle$. In the first interval, we used the Schechter parameters found by Loveday et al. (1992) for the local luminosity function in the Stromlo-APM survey; $M_{b_{\rm J}} = -19.5$, $\alpha = -0.97$ and $\phi^* = 0.014$ Mpc^{-3}. For the three other intervals, we used $M^*_{AB}(B) = -21.04$, -20.83 and -21.24 as found by Lilly et al. for their 'All' colour sample in the CFRS. We also fixed α at -0.89 in these three redshift intervals, since the slopes reported by Lilly et al. at these redshifts are seen to vary a lot, which presumably is not a real evolutionary effect. Since the CFRS luminosity function is defined over a narrow magnitude range, the faint-end slope may have high uncertainties. For example, in the redshift range $\langle 0.5,0.75\rangle$ that we are most interested in here, and at luminosities from $M_{AB}(B) = -19.7$ to -22.9, Lilly et al. find that $\alpha = -0.5$. The faintest absolute magnitude in this range corresponds to ≈ -21 in R, whereas our completeness limit in R corresponds to ≈ -20 at $z = 0.6$, so our data are approximately one magnitude deeper. We therefore chose $\alpha = -0.89$ since this is the slope they find for the total luminosity function from $z = 0.0$ to 1.3.

The four luminosity function segments were integrated with respect to luminosity down to the completeness limit of our data at the average redshift in each interval. The completeness magnitudes in R and I were found by applying K-corrections and galaxy colours of an Sa galaxy listed as a function of redshift by Rocca-Volmerange & Guiderdoni (1988) and Guiderdoni & Rocca-Volmerange (1988). The characteristic magnitudes in each interval were transformed from B_{AB} to R and I by first using that $B_{AB} = B - 0.17$ (Oke 1972), and thereafter assuming $B - V = 0.74$, $V - R = 0.68$ and $R - I = 0.57$ which are the colours of an Sa galaxy model at $z = 0$ (Guiderdoni & Rocca-Volmerange 1988). The $M^*_{b_{\rm J}}$ magnitude in the lowest redshift interval was converted to B by assuming $b_{\rm J} = B - 0.09$ (Metcalfe et al. 1991).

Then the integration was carried out over redshift, from $z = 0.0$ to 1.0. From these approximate calculations we constructed number counts that were subsequently matched to the observed counts by varying the ϕ^*'s of each segment until a minimum in χ^2 was reached. For the I-band data we found it sufficient to use the same scaling for all intervals, and the best fit was obtained with $\phi^* = 0.0052$ Mpc^{-3} for the $\langle 0.5, 0.75\rangle$ interval. In R, very little adjustment was needed in ϕ^* to fit the data, and for the $\langle 0.5, 0.75\rangle$ interval we found a best fit with $\phi^* = 0.0072$ Mpc^{-3}.

To normalize $B_{\rm gq}$, we evaluated $\Phi(m_{\rm lim}, z)$ for every quasar field by integrating the Schechter function from $-\infty$ to an absolute magnitude corresponding to the completeness limit at the quasar redshift. The absolute limiting magnitude in every quasar frame was found by converting the apparent completeness limit to an absolute magnitude using K-corrections for a hot E/S0 galaxy (Rocca-Volmerange & Guiderdoni 1988). Typical values obtained for the integrated luminosity function were $\Phi(m_{\rm lim}, z) \sim 0.005$–$0.007$ Mpc^{-3}.

The results of the computations of $B_{\rm gq}$ are shown in Table 4. The errors in $A_{\rm gq}$ and $B_{\rm gq}$ were calculated according to

$$\frac{\Delta A_{\rm gq}}{A_{\rm gq}} = \frac{\Delta B_{\rm gq}}{B_{\rm gq}} = \frac{[(N_{\rm tot} - N_{\rm b}) + 1.3^2 N_{\rm b}]^{1/2}}{N_{\rm tot} - N_{\rm b}} \qquad (3)$$

(Yee & López-Cruz 1999) and reflect the errors in the galaxy counts on the quasar and background images, but not uncertainties in the luminosity function. (Yee & López-Cruz also argue that the inverse of this error underestimates the statistical significance of excess galaxy counts which may be better represented by $(N_{\rm tot} - N_{\rm b})/1.3\sqrt{N_{\rm b}}$.) In Table 4, $B_{\rm gq}$ found from both the raw and the corrected counts are shown. On average the corrected $B_{\rm gq}$'s are larger since these were deduced from deeper counts, in some cases down to $R = 24.5$ (for MRC 0144−058, MRC 0159−117 and 7C 3066). In cases where the quasar and background fields had different completeness limits, we took the brightest magnitude as the limit. Some fields could not be pushed

further with regard to the limiting magnitude, so these are left as 'unchanged'. The *HST* images were also not corrected.

The counting of galaxies should not be done either too far below or too far above M^* of the surrounding galaxy cluster in order to obtain a reliable result. At faint magnitudes the background counts rise faster than the associated galaxy counts, and a possible excess may drown in the background. Yee & López-Cruz (1999) showed that if the appropriate luminosity function is used to normalize the counts, i.e. that the ϕ^* of this luminosity function can reproduce the observed background counts, then the best results are obtained by counting down to a magnitude between $M^* + 1$ and $M^* + 3$. As far as possible, we have attempted to reach $M^* + 2$, and our completeness magnitudes of $R = 23.5$ and $I = 23.0$ correspond to $M_R \approx -20.5$ and $M_I \approx -20.8$ at redshifts 0.6 and 0.7 (assuming *K*-corrections of approximately 1 and 0.5 mag). Provided that M^* of the associated galaxies is approximately the same as the one in the field given by Lilly et al. (1995), we have reached deep enough in all fields, except 7C 3222 and 7C 3450. These two fields have shallower completeness limits (imaged at the 107-inch telescope) of 22.5 in *R* and 21.5 in *I*, corresponding to $M_R^* \approx -21.5$ and $M_I^* \approx -22.4$, i.e. not as deep as $M^* + 1$. Using the corrected counts, we go half a magnitude deeper and should therefore be on the faint side of $M^* + 1$.

6.3 Comparison with previous work

We may compare with YG87 and EYG91 who also quantified quasar environments in terms of $B_{\rm gq}$. The greatest difference between their and our analysis is the method used for choosing the appropriate luminosity function for normalizing $B_{\rm gq}$. Since determinations of the field galaxy luminosity function at higher redshifts were not available to them, they used local luminosity functions from the literature which they fitted to the observations in two steps. First, they added an evolution in M^* that matched the observed luminosity function of the associated galaxies. A possible risk with this is that too much evolution may be added to M^* if the quasar fields are contaminated by foreground galaxies. This approach also assumes that the field and cluster luminosity function evolve together. Secondly, they scaled ϕ^* of the evolved local luminosity function to match the observed background counts.

For $\langle z \rangle = 0.6$, YG87 used $M_r^* = -21.55$, $\alpha = -1.2$ and $\phi^* = 0.0058\,{\rm Mpc}^{-3}$ ($q_0 = 0.5$), and EYG91 used $M_r^* = -21.73$, $\alpha = -1.0$ and $\phi^* = 0.0027\,{\rm Mpc}^{-3}$ ($q_0 = 0.02$). To compare the characteristic magnitudes, we transformed from *r* to *R* by assuming $r - R \approx 0.43$ (Fukugita, Shimasaku & Ichikawa 1995) and applied *K*-corrections for a hot E/S0 galaxy (Guiderdoni & Rocca-Volmerange 1988) since YG87 and EYG91 give M_r^* in the observed waveband. We found $M_R^*({\rm YG87}) = -22.98$ and $M_R^*({\rm EYG91}) = -22.85$ ($q_0 = 0.5$). By adding a colour of $R - I = 0.78$ to the *R* mag, we obtained $M_I^*({\rm YG87}) = -23.76$ and $M_I^*({\rm EYG91}) = -23.63$. It therefore seems that we have used an M^* that is approximately one mag fainter than in both of these studies, and also a ϕ^* that is larger. A fainter characteristic magnitude will lower the value of the integrated luminosity function, thereby bringing $B_{\rm gq}$ up by a small amount, but at the same time, a larger value of ϕ^* will increase the number of galaxies above the limiting magnitude, with the result that $B_{\rm gq}$ decreases.

The mean $B_{\rm gq}$ for the quasar fields in our sample is $265\,{\rm Mpc}^{1.77}$ with an error in the mean of $74\,{\rm Mpc}^{1.77}$ (from a combination of intrinsic dispersion in $B_{\rm gq}$ and measurement error). With 5C 6.189 excluded, this becomes $249 \pm 75\,{\rm Mpc}^{1.77}$. To see how the choice of different luminosity functions affected our measurements, we recomputed $B_{\rm gq}$ with both YG87's and EYG91's luminosity functions. In the first case, we obtained overall lower values of $B_{\rm gq}$; the mean was found to be $185 \pm 57\,{\rm Mpc}^{1.77}$. In the second case, we transformed to a $q_0 = 0.02$ cosmology for consistency, and found a better agreement and the mean $B_{\rm gq}$ was $257 \pm 77\,{\rm Mpc}^{1.77}$. The correlation amplitude is rather insensitive to q_0, and using $q_0 = 0.02$ has very little effect on $B_{\rm gq}$. For example, at $z = 0.5$, $B_{\rm gq}$ is smaller by a factor of $\sim$1.15 if $q_0 = 0.02$ instead of 0.5.

We have one field in common with Yee & Ellingson (1993) with which we may compare more directly. They report that $B_{\rm gq}$ in the MRC 0405−123 field is 905 ± 277, whereas we find $875 \pm 176\,{\rm Mpc}^{1.77}$. When we recalculated $B_{\rm gq}$ with EYG91's luminosity function, we found 1006 ± 231 for this field, and with YG87's luminosity function as normalization, we obtained $647 \pm 96\,{\rm Mpc}^{1.77}$. There thus seems to be very good agreement between our and the Yee & Ellingson result for this field, and in particular that this quasar lies in a relatively rich cluster.

In Fig. 4 we have plotted our $B_{\rm gq}$ measurements obtained from the corrected counts together with $B_{\rm gq}$ for YG87's and EYG91's quasar fields as a function of redshift. In this figure, we have also added quasar fields reported by Yee & Ellingson (1993) that do not overlap with sources from YG87 and EYG91 (referenced in table 1 in Yee & Ellingson as coming from Yee & Green 1984 and from unpublished CTIO and CFHT images). We used photometric information available in the NASA/IPAC Extragalactic Database (NED) to find the spectral index of the literature sources, and found that some of them were flat-spectrum quasars. These were omitted in Fig. 4, since we only want to compare with other steep-spectrum sources. (We also found that three of the quasars, 0208−018, 0438−165 and 0449−183, listed as radio-loud in table 2 of EYG91, are radio-quiet according to the definition by Kellerman et al. (1989). These were also ignored.) It seems that there are no systematic differences in our estimates of $B_{\rm gq}$ and the other estimates from the literature. The majority of the literature quasar fields have amplitudes below $500\,{\rm Mpc}^{1.77}$, a trend which is present also in our fields, and the overall impression from Fig. 4 is that the correlation amplitudes from the different samples are

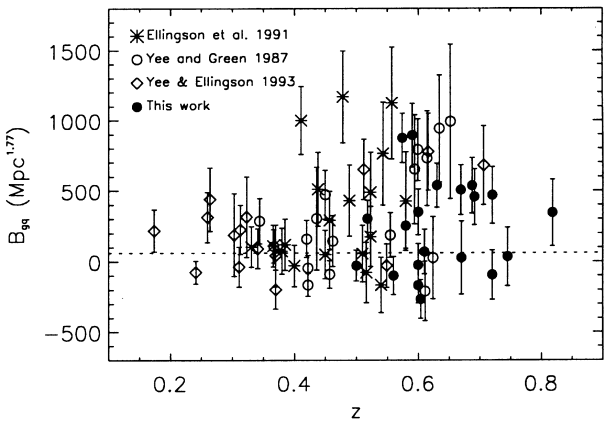

Figure 4. The cross-correlation amplitudes from this work, derived from the corrected counts, plotted together with $B_{\rm gq}$ for steep spectrum radio-loud quasars from the literature. The galaxy–galaxy correlation amplitude for low-*z* galaxies in the field, $B_{\rm gg} \approx 60\,{\rm Mpc}^{1.77}$ (Davis & Peebles 1983), is shown as a dotted line across the plot.

consistent with each other and fall approximately in the same range. We do not see any redshift dependence in B_{gq}, either in our own sample or in the combined sample, as shown in Fig. 4. Adding the flat-spectrum quasars seems to make no substantial difference to the plot, and it is difficult to see any significant trend in the flat-spectrum population alone.

6.4 Comparison with other two-point correlation functions

The average B_{gq} for our sample, $265 \pm 74\,\mathrm{Mpc}^{1.77}$, is significantly larger than the galaxy–galaxy correlation amplitude in the field measured both locally and at higher redshifts. The local galaxy–galaxy correlation function, $\xi_{gg}(r) = (r/r_0)^{-\gamma}$, has been measured by several investigators (e.g. Davis & Peebles 1983; Loveday et al. 1995; Guzzo et al. 1997) and results emerging from these studies show that $r_0 \approx 10\,\mathrm{Mpc}$ and $\gamma \sim 1.7$, i.e. that $B_{gg} \approx 60\,\mathrm{Mpc}^{1.77}$ ($H_0 = 50\,\mathrm{km\,s^{-1}\,Mpc^{-1}}$). Written as a correlation length, our mean B_{gq} corresponds to $r_0 = 23.4\,\mathrm{Mpc}$.

Several attempts have been made to measure ξ_{gg} up to $z \approx 0.5$, but the results so far seem to disagree to some extent. Le Fèvre et al. (1996), using the CFRS, find evidence for a decrease in the correlation length toward higher redshifts with $r_0 = 2.66\,\mathrm{Mpc}$ and $\gamma = 1.64$ at $z = 0.53$. Hudon & Lilly (1996) find $r_0 = 3.78\,\mathrm{Mpc}$ at $z = 0.48$. On the other hand, Carlberg et al. (1998) and Small et al. (1999) find no evidence for evolution between $z \approx 0.1$ and 0.6, and Small et al. get a correlation length of $r_0 = 7.4\,\mathrm{Mpc}$ at $z \sim 0.3$. Nevertheless, the values we are measuring for B_{gq} are larger than the observed galaxy–galaxy correlation amplitude at both higher and lower redshifts, and show that we have clearly detected enhancements in the galaxy density around the quasars.

We can also compare our B_{gq} values with B_{cg}, the amplitude of the cluster–galaxy cross-correlation function, ξ_{cg}. Lilje & Efstathiou (1988) measured ξ_{cg} on scales down to 0.2 Mpc using Abell clusters and the Lick galaxy counts. They found that ξ_{cg} was well fit by the same functional form as ξ_{gg}, but with $\gamma = 2.2$ and a correlation length $r_0 = 17.6\,\mathrm{Mpc}$. Subsequently, Croft, Dalton & Efstathiou (1999) have shown that this is also a good approximation to ξ_{cg} obtained from the independent Stromlo-APM galaxy and APM cluster redshift surveys on scales of 0.2 to >20 Mpc. Prestage & Peacock (1988, 1989), Andersen & Owen (1994) and Yee & López-Cruz (1999) have examined B_{cg} measured in 1, 1–1.5 and 0.5 Mpc circles, respectively, as a function of cluster richness, all assuming $\gamma = 1.77$. Comparison of these measurements of B_{cg} with the one of Lilje & Efstathiou reveals some discrepancies, presumably caused by systematic differences in the measurements and scatter in the richnesses of the clusters observed. To compare the Lilje & Efstathiou function with the rest, we evaluated ξ_{cg} at a radius of 0.5 Mpc, then converted to B_{cg} assuming $\gamma = 1.77$. This comes out to $B_{cg} = 740\,\mathrm{Mpc}^{1.77}$. Prestage & Peacock estimate $B_{cg} \approx 690\,\mathrm{Mpc}^{1.77}$ for an Abell class 1 cluster, and Andersen & Owen $\approx 615\,\mathrm{Mpc}^{1.77}$, both broadly consistent with the Lilje & Efstathiou function (which was calculated for clusters with Abell richness class ≥ 1). In contrast, Yee & López-Cruz using CCD data find a median $B_{cg} \approx 950\,\mathrm{Mpc}^{1.77}$ for an Abell class 1 cluster. We have decided to take the mean for Abell class 1 to be $740\,\mathrm{Mpc}^{1.77}$ simply on the basis that more clusters were involved in the Lilje & Efstathiou study, and note that this is more likely to be an overestimate than an underestimate as clusters richer than Abell class 1 were included. We have two quasar fields that have B_{gq} larger than this value, which suggests that a few quasars at $0.5 < z < 0.8$ are found in clusters of approximately Abell class 1 or greater, but that most are in poorer groups or clusters.

We believe that we have not overestimated the richness, since we also find fields with negative B_{gq}. However, a small or negative B_{gq} need not mean that there are no galaxies associated with the quasar, but simply that the associated galaxies are lost in the fluctuations of the background counts.

6.5 Calculation of $N_{0.5}$

We also calculated $N_{0.5}$ (Hill & Lilly 1991) for each quasar field by counting the number of galaxies within the 0.5-Mpc radius with magnitudes ranging from m_g to $m_g + 3$, where m_g is the typical magnitude of a radio galaxy (equation 2) at the quasar redshift. The average number of galaxies within the same magnitude range in the background control images was subtracted from the counts in the quasar fields. The estimates of $N_{0.5}$ obtained in this manner are listed in Table 4 in the last column. Since the 7C 3222 and 7C 3450 fields from the 107-inch telescope at the McDonald Observatory are not deep enough for $m_g + 3$ to be brighter than the completeness limit, we have calculated $N_{0.5}$ from m_g down to the completeness limit (21.5 in I and 22.5 in R).

Although this is a measurement intended for fields around radio galaxies, it seems to give a good estimate of the richness in quasar fields since we find an overall correspondence between B_{gq} and $N_{0.5}$, as shown in Fig. 5. In this figure, large values of B_{gq} are seen to pair rather well with large numbers of $N_{0.5}$, and fitting a straight line gives a best fit of $B_{gq} = (37.8 \pm 10.9)N_{0.5}$, slightly steeper than the relation, $B_{gg} = 30N_{0.5}$, found by Hill & Lilly for radio galaxies, but still a good agreement considering that we have only estimated m_g from a magnitude–redshift relation. There are a couple of fields with higher $N_{0.5}$ that do not follow the trend as nicely as the rest of the fields (7C 3814 and MRC 0144−058). Some fluctuations are expected, as $N_{0.5}$ is not as deep a measurement as B_{gq}, and also the number of field galaxies in the quasar images fluctuates to some level.

In Fig. 6, we plot $N_{0.5}$ for quasars in our sample together with $N_{0.5}$ obtained for radio galaxies by Hill & Lilly (1991). (Hill & Lilly also assume $H_0 = 50\,\mathrm{km\,s^{-1}\,Mpc^{-1}}$ and $q_0 = 0.5$). Our values of $N_{0.5}$ seem to lie approximately in the same range as those obtained by Hill & Lilly, although at the higher redshift end, Hill & Lilly's values for a few sources are larger.

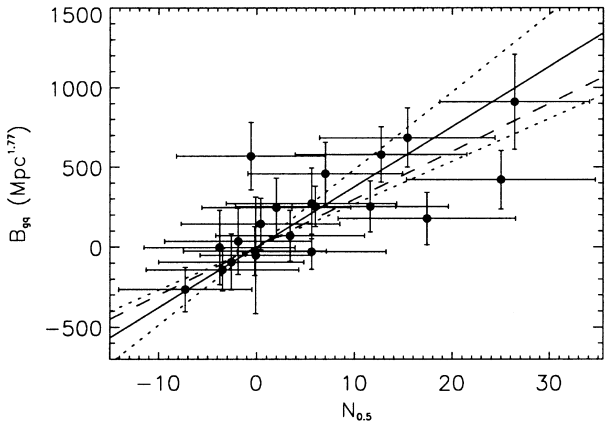

Figure 5. B_{gq} plotted versus $N_{0.5}$. The solid and the dotted lines show the best fit of $B_{gq} = (37.8 \pm 10.9)N_{0.5}$. The dashed line is the relation for radio galaxies from Hill & Lilly (1991), $B_{gg} = 30N_{0.5}$.

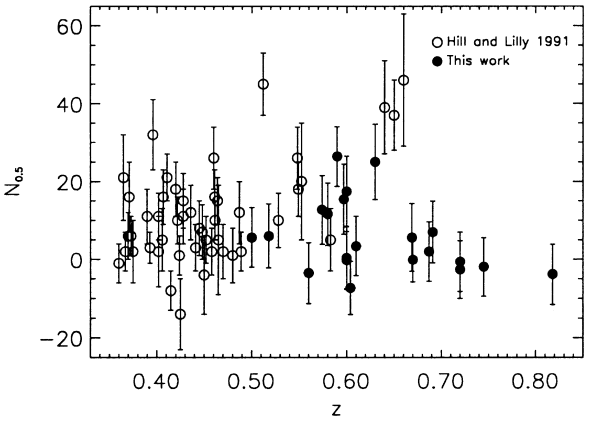

Figure 6. $N_{0.5}$ for the sample of radio galaxies by Hill & Lilly (1991) (open circles) plotted together with $N_{0.5}$ for the quasars in our sample (filled circles).

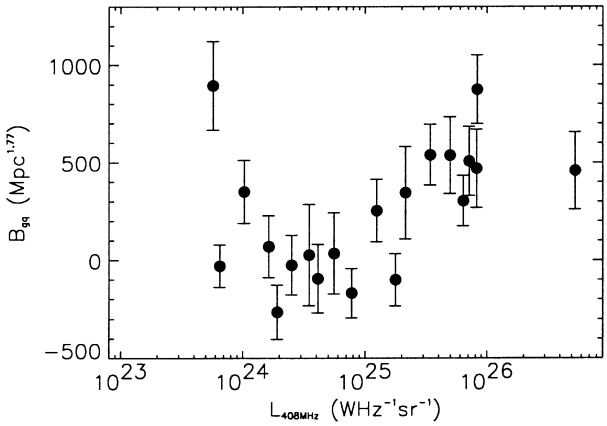

Figure 7. $B_{\rm gq}$ plotted as a function of radio luminosity at 408 MHz.

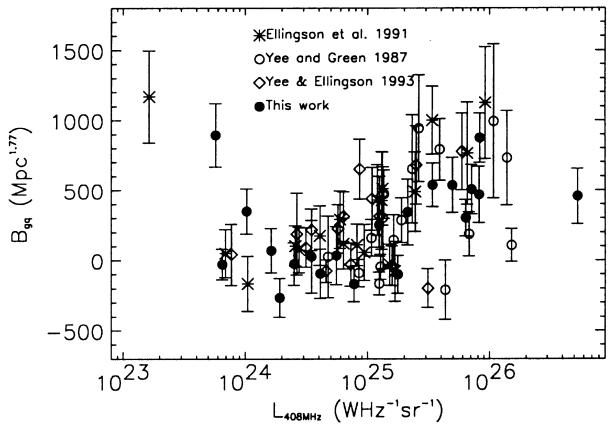

Figure 8. $B_{\rm gq}$ versus radio luminosity for objects in our sample together with steep-spectrum quasars from the literature.

7 RADIO LUMINOSITY AND REDSHIFT DEPENDENCES OF THE CLUSTERING STRENGTH

In order to examine whether the strength of galaxy clustering around the quasars is determined by epoch or radio luminosity, we looked for correlations between $B_{\rm gq}$, redshift and radio luminosity.

In Fig. 7 we have plotted $B_{\rm gq}$ as a function of radio luminosity at 408 MHz, $L_{408\,\rm MHz}$. The figure suggests that a positive correlation between $B_{\rm gq}$ and radio luminosity may be present; at least there seems to be more of a trend with radio luminosity than with redshift if we compare with Fig. 4.

Our sample is rather small and covers a relatively narrow redshift range, we therefore included the measurements of quasar environments down to $z \approx 0.2$ from YG87, EYG91 and Yee & Ellingson (1993). We used photometry from the NED to find flux densities and spectral indices to calculate radio luminosities for the literature sources. In a few cases where the source was not available in NED, we used the NRAO VLA Sky Survey (NVSS) (Condon et al. 1998). Since one of the aims was to investigate radio luminosity dependences, we excluded sources that were flat-spectrum quasars (nine sources in EYG91 and five from Yee & Ellingson, as well as 5C 6.189 from our own sample), leaving us with a total of 71 radio-loud steep-spectrum quasars. (The three sources in table 2 of EYG91 found to be radio-quiet were also omitted.)

In Fig. 8, we have plotted the $B_{\rm gq}$'s for all sources as a function of radio luminosity. To examine whether there are any trends in the data, we divided the quasars into redshift and luminosity sub-samples and computed the mean $B_{\rm gq}$ in each sub-sample. The result of this is shown in Table 5.

The mean $B_{\rm gq}$ for all quasar fields in our sample, 249 ± 75, is seen to be consistent with the mean of 304 ± 51 for the literature sources, and the mean of $289 \pm 42\,{\rm Mpc}^{1.77}$ for the combined samples. The fact that the normalization of $B_{\rm gq}$ was done in a self-consistent manner, both by us and the other investigators, is reassuring when we utilize their results in analyses like this. We also bear in mind the good agreement about the richness of the MRC 0405−123 field. As seen in Table 5, the literature samples show a higher $\langle B_{\rm gq}\rangle$ in the $z \geq 0.5$ sub-sample than in the lower redshift sub-sample, and we interpret this as the epoch-dependent evolution in $B_{\rm gq}$ claimed by Yee & Ellingson (1993). The mean $B_{\rm gq}$ for the combined samples is also seen to be larger in the high-redshift sub-sample, but here the difference is smaller. However, the difference in the mean $B_{\rm gq}$ for the low and high radio luminosity sub-samples is more pronounced. Here, we found $\langle B_{\rm gq}\rangle = 136 \pm 72$ at low luminosities and $\langle B_{\rm gq}\rangle = 353 \pm 49\,{\rm Mpc}^{1.77}$ at high luminosities. The sources in our own sample gave a similar result, but with an even larger difference, $\langle B_{\rm gq}\rangle = 107 \pm 112$ at low luminosities and $365 \pm 89\,{\rm Mpc}^{1.77}$ at high luminosities. The division between the high- and low radio luminosity sub-samples was set at $L_{408\,\rm MHz} = 10^{24.75}\,{\rm W\,Hz^{-1}\,sr^{-1}}$, which corresponds to the break in the radio luminosity function.

Table 5. Mean $B_{\rm gq}$ for sub-samples of steep-spectrum quasars. The results for our sample, the literature samples (YG87; EYG91; Yee & Ellingson 1993) and all samples combined, are shown. Radio luminosity, $L_{408\,\rm MHz}$ is given in ${\rm W\,Hz^{-1}\,sr^{-1}}$ and the unit of $B_{\rm gq}$ is ${\rm Mpc}^{1.77}$. The number of objects in each sub-sample is denoted by N.

Sub-sample	Our $\langle B_{\rm gq}\rangle$	N	Literature $\langle B_{\rm gq}\rangle$	N	Our + literature $\langle B_{\rm gq}\rangle$	N
All quasars	249 ± 75	20	304 ± 51	51	289 ± 42	71
$z < 0.5$		0	211 ± 53	31	211 ± 53	31
$z \geq 0.5$	249 ± 75	20	450 ± 94	20	349 ± 61	40
$L_{408} < 10^{24.75}$	107 ± 112	9	158 ± 97	12	136 ± 72	21
$L_{408} \geq 10^{24.75}$	365 ± 89	11	349 ± 59	39	353 ± 49	50

In order to quantify the trends better, and to disentangle the effects that redshift and radio luminosity may have on $B_{\rm gq}$, we

followed the approach of Yates et al. (1989) and computed the Spearman partial rank correlation coefficient, $r_{AX,Y}$, for the different samples. The $r_{AX,Y}$ statistic is defined as

$$r_{AX,Y} \equiv \frac{r_{AX} - r_{XY}r_{YA}}{[(1 - r_{XY}^2)(1 - r_{YA}^2)]^{1/2}},$$

where r_{AX}, r_{XY} and r_{YA} are the usual Spearman rank correlation coefficients. The $r_{AX,Y}$ statistic is a number between -1 and $+1$ and serves as an indicator of the trend of large values of A to be paired with large values of X when the effect of the third variable, Y, has been removed. A value of $(-)+1$ indicates a perfect (anti)correlation between A and X at constant Y. For N data points, the significance level of $r_{AX,Y}$ is

$$D_{AX,Y} = \frac{1}{2}(N-4)^{1/2} \ln\left[\frac{1 + r_{AX,Y}}{1 - r_{AX,Y}}\right]$$

(Macklin 1982), and is approximately normally distributed about zero with unit variance if the null hypothesis, that the A–X correlation arises entirely from those of Y with A and X separately, is true. Here, we let A, X and Y be combinations of $B_{\rm gq}$, $L_{408\,\rm MHz}$ and z, so that the correlation between, e.g. $B_{\rm gq}$ and $L_{408\,\rm MHz}$ with z held constant can be found. By using this statistic, we hope to determine whether there exists a correlation in $B_{\rm gq}$ with either z (independent of $L_{408\,\rm MHz}$) or $L_{408\,\rm MHz}$ (independent of z).

The Spearman partial rank correlation coefficients were computed in three different cases: our own sample, the literature samples (YG87+EYG91+Yee & Ellingson) and the samples combined. The resulting correlation coefficients and their significances are shown in Table 6. The table contains two cases; the first three lines show the Spearman coefficients calculated by including all steep-spectrum quasars, whereas in the lower part we have included only those steep-spectrum sources which have extended radio morphologies, i.e. we have excluded quasars that have sizes $r < 30$ kpc and are classified as CSS sources. The CSS sources may not sample the large-scale density distribution outside the ISM of the host galaxy, and therefore might not be expected to follow the same trends as the rest of the source population. The Spearman statistic without the CSS sources remains almost unchanged, however.

The numbers in Table 6 seem to indicate a weak, but significant, dependence of $B_{\rm gq}$ on radio luminosity. Both in our sample and in the combined samples, it is the most significant correlation, and it is strongest when all the samples are combined, giving $r_{B_{\rm gq}L_{408},z} = 0.47$ with a 3.7σ significance when the CSS sources are excluded. In the literature sample, it is the correlation between radio luminosity and redshift that dominates. This makes it difficult to interpret any changes in $\langle B_{\rm gq}\rangle$ within the two sub-samples, and especially we cannot be certain that there is a true evolution with redshift. However, both in our sample and in the combined samples $r_{B_{\rm gq}z,L_{408}}$ is negligible and insignificant compared to $r_{B_{\rm gq}L_{408},z}$. The result of this analysis is therefore suggestive of a radio luminosity dependence in $B_{\rm gq}$, and we believe that there is no evidence for a redshift dependence as has been claimed by, e.g. YG87 and Yee & Ellingson (1993).

Table 6. Spearman partial rank correlation coefficients for the three different samples. Our sample, samples from the literature (YG87; EYG91; Yee & Ellingson 1993), and our sample combined with the literature samples. The lower half of the table shows the results of the correlation analysis when the compact steep-spectrum sources were excluded. The numbers in parenthesis behind the correlation coefficients are significances.

Sample	N	$r_{B_{\rm gq}L_{408},z}$	$r_{B_{\rm gq}z,L_{408}}$	$r_{L_{408}z,B_{\rm gq}}$
Our	20	0.41 (1.7σ)	0.02 (0.1σ)	0.22 (0.9σ)
Literature	51	0.26 (1.8σ)	0.19 (1.3σ)	0.39 (2.8σ)
Combined	71	0.39 (3.4σ)	0.10 (0.8σ)	0.23 (1.9σ)
Our	14	0.60 (2.2σ)	-0.18 (-0.6σ)	0.41 (1.4σ)
Literature	44	0.27 (1.8σ)	0.14 (0.9σ)	0.39 (2.6σ)
Combined	58	0.47 (3.7σ)	0.02 (0.1σ)	0.22 (1.6σ)

We may consider that if our estimates of $B_{\rm gq}$ are systematically different from the others, then a bias could be introduced, but we do not think that this is the case. First, the agreement about the value of $B_{\rm gq}$ for the field around MRC 0405−123 is very good. Secondly, the trends within our own sample are the same as those found for the combined samples. Thirdly, the $B_{\rm gq}$ estimates, determined from the raw counts in our data, also give a significant correlation between $B_{\rm gq}$ and $L_{408\,\rm MHz}$, and produce the same trend as above when we combine with the literature sources. Fourthly, the result of the correlation analysis using the recomputed $B_{\rm gq}$'s with EYG91's luminosity function as normalization also show that the $B_{\rm gq}$–$L_{408\,\rm MHz}$ correlation is the strongest. However, we may note, as mentioned by Yates et al. (1989), that $r_{B_{\rm gq}z,L_{408}}$ computed for a combination of samples that have been analysed by different authors should be viewed with some caution since differences in $\Phi(m_{\rm lim},z)$ and the assumed cosmology may introduce spurious effects.

8 DISCUSSION

8.1 Comparison with radio galaxy environments

Previously, studies of radio galaxies spanning a wide range in radio luminosity at a given redshift have found that the richness of radio galaxy environments is increasing with redshift, but does not correlate with radio luminosity (Hill & Lilly 1991; Allington-Smith et al. 1993). It would be intriguing if a correlation between clustering strength and radio luminosity was found for radio-loud quasars but not for radio galaxies. The 'Unified Scheme' for radio-loud AGN predicts that these are the same type of object viewed from different angles, so the richness of the environments should have the same behaviour with radio luminosity and redshift. Why, then, are the radio quasars apparently different to the radio galaxies?

First, we consider the possibility that selection effects are responsible. Our sample was initially chosen such as to consist of one low and one high radio luminosity sub-sample. The sources in these two sub-samples were selected randomly from the complete radio/optical flux-limited 7CQ (Riley et al. 1999) and MAQS samples (Serjeant 1996), on the basis of redshift, right ascension and declination. The only possible source of bias would be a selection effect which leads us to give preference to less dense environments at low radio luminosities (the 7CQ quasars) and more dense environments at high radio luminosities (the MAQS quasars).

This selection effect is possible if the radio luminosity of a quasar is controlled *both* by the environmental richness/density ($B_{\rm gq}$) and the bulk kinetic power in the radio jets (optical luminosity). We discuss this in greater detail in Section 8.3. The 7CQ sample has a relatively bright optical flux limit, which selects sources with unusually high optical luminosities for their radio luminosities. The objects that we miss in the 7CQ survey are therefore optically faint with low jet powers, so their radio luminosity must be enhanced by a dense environment. We may therefore be biased against optically faint quasars in dense

environments and favour quasars in low-density environments instead, characterized by low B_{gq}'s.

In the MAQS sample, where the optical flux limit is faint, the effect would be to favour quasars in dense environments, i.e. high B_{gq}'s. A faint quasar with weak jets in a dense environment can have the same radio luminosity as an optically bright quasar in less dense environments since the powerful jets of the latter will enhance the radio luminosity. Due to the steep increase of the optical quasar luminosity function towards low luminosities, we have more optically faint sources than we have bright sources, and since the sample also is radio flux-limited, we miss optically faint sources in low-density environments. The preference is thus given to optically faint sources in high-density environments having high B_{gq}'s.

In the YG87 and EYG91 samples similar effects may operate, as most radio quasar samples are selected with an optical flux limit close to the POSS-I plate limit, but they are harder to quantify as the samples are not complete.

A second possible explanation is that we are not comparing like with like, especially at radio luminosities close to the break in the radio luminosity function. Recently, Laing et al. (1994) found evidence for two different types of radio galaxies: low-excitation narrow-line radio galaxies (LEG), appearing as typical radio galaxies in radio, but with weak optical emission lines that commonly have low excitation, and high-excitation narrow-line radio galaxies (HEG) with strong, high-ionization emission lines. The HEGs are thought to be the objects which unify with quasars, whereas the LEGs, unless seen with their jets pointing almost directly along the line of sight (when they are seen as BL Lacertae objects) are radio galaxies at all orientations since no broad lines are observed. If the clustering properties of HEGs and LEGs differ, then a sample of radio galaxies with a mix of both HEGs and LEGs (such as that of Hill & Lilly 1991) must be considered less uniform and difficult to compare with quasars.

8.2 The clustering properties of quasars and radio galaxies

Because our quasars are typically in poor clusters, we can estimate their clustering (i.e. B_{qq}) by assuming the ratio $B_{qq}/B_{qc} = B_{cc}/B_{cg} \approx 1.7$, where B_{cc} and B_{cg} are the cluster–cluster and cluster-galaxy correlation amplitudes respectively, from Croft et al. (1997, 1999). This gives a correlation amplitude for radio-loud quasars of $\approx 490\,\mathrm{Mpc}^{1.77}$ (after correcting all numbers to a $\gamma = 1.77$ at 0.5 Mpc for consistency). This is large compared to low redshift radio galaxies measured by Peacock & Nicholson (1991) who obtain $B_{g^*g^*} \approx 240\,\mathrm{Mpc}^{1.8}$, and the faint radio galaxies in the FIRST (Far Infrared and Submillimetre Space Telescope) survey, for which Magliocchetti et al. (1998) estimate $B_{g^*g^*} \approx 220\,\mathrm{Mpc}^{1.8}$. Both the Peacock & Nicholson and the Magliocchetti et al. studies are dominated by lower luminosity objects than in our quasar sample, further evidence of a radio luminosity and/or redshift dependence of clustering strength. Also pertinent to this is the 2-degree Field (2dF) QSO Redshift Survey (Croom et al. 1999) currently underway at the Anglo-Australian Telescope, which will, in due course, measure the clustering of high-z radio-quiet quasars directly, and also determine the evolution in the clustering strength with redshift.

8.3 The link between cluster richness and radio luminosity

Does our discovery of a correlation between radio luminosity and B_{gq} imply that environment is the primary factor in controlling radio luminosity? If so there are at least three ways in which such a situation could come about: (1) the environment determines the bulk kinetic power in the radio jets, Q, through a correlation of cluster richness with the black-hole mass in the central group/cluster galaxy; (2) the environment determines Q through more AGN fuel being available in richer environments, or (3) Q is independent of environment and similar for all radio sources, with the radio luminosity being determined solely by the density into which the source expands.

The argument in favour of possibility (1) is based on the correlation between black hole mass and the mass of the spheroidal component suggested by Kormendy & Richstone (1995) and Magorrian et al. (1998). This implies that the giant elliptical hosts of radio galaxies and quasars should have high black-hole masses, $\sim 10^8$–$10^9\,\mathrm{M}_\odot$. If the jets are powered by accretion then it seems reasonable to expect that the maximum accretion rate is proportional to the Eddington rate, and hence the black-hole mass. So more massive galaxies should power more luminous radio sources. These massive galaxies will always prefer richer environments, and the correlation between luminosity and cluster richness may just reflect an increasing mass of the host galaxy (and hence of the black hole). The principal argument against this is the lack of any obvious correlation of host galaxy luminosity with radio luminosity, at least out to $z \sim 0.6$ (Serjeant et al. 1997), although there is a suggestion that by $z \sim 1$ the hosts of radio galaxies do show such a trend (Roche, Eales & Rawlings 1998).

The possibility (2), that fuelling of the AGN determines its environment, is discussed by Ellingson, Green & Yee (1991). A group or poor cluster environment may be ideal for the fuelling of a black hole, as encounters will be more common than in the field, but will be of low enough relative velocity to disrupt the interacting galaxies and cause gas to flow into the centre. Lake, Katz & Moore (1998), however, have also demonstated that galaxy harassment (frequent high-speed galaxy encounters) in relatively high velocity dispersion clusters may be an efficient mechanism for transporting gas to the centre of galaxies. If this mechanism is responsible for fuelling the black hole it may explain the correlation of radio luminosity with cluster richness, but cannot explain why low-power FR I radio sources are also found in rich clusters.

Possibility (3) is suggested by models of radio sources which show that the radio luminosity of an expanding radio source is primarily determined by the bulk kinetic power in the radio jet, Q, and the environmental density, ρ, as a function of distance from the nucleus, r, usually parametrized by

$$\rho \propto \rho_0 (a_0/r)^\beta,$$

where a_0 and ρ_0 are the characteristic radius and density, and β is a power-law slope. Kaiser, Dennett-Thorpe & Alexander (1997) show how the track of the expanding radio source on the radio luminosity–size diagram is determined by different values of these parameters. The small dispersion in galaxy mass (and therefore perhaps black-hole mass) of radio source host galaxies might suggest that, if all radio sources are accreting matter at the same fraction of the Eddington rate, the values of Q should be similar for all radio sources. However, it is clear from the models that radio luminosity is also strongly dependent on the mean environmental density. This is because objects located in dense gaseous haloes have lower losses due to adiabatic expansion, and the transfer of AGN power into radiation thus becomes very efficient due to the reduced expansion losses. Indeed, Barthel &

Arnaud (1996) use the case of Cygnus A, which is in such an environment, to argue that environmental density *controls* radio source luminosity. Consistent with this, Hutchings et al. (1996) claim to find a weak, positive correlation between lobe luminosity of quasars and $B_{\rm gq}$.

On the other hand, a relation between radio and [O III] emission-line luminosity is observed (Rawlings & Saunders 1991; Willott et al. 1999). The [O III] λ5007 luminosity is believed to be powered by UV radiation from the nucleus (for a different view, see Dopita & Sutherland 1995), and these observations thus argue that radio luminosity is primarily determined by jet kinetic power. Serjeant et al. (1998) also find that the radio and optical luminosity of quasars correlate. If both are related to the luminosity of the AGN powered by accretion, then this also suggests that jet power, not environmental density, is the most important factor in determining the radio luminosity.

To investigate the possible implications of (3) for our study though, we have constructed a simple model of how radio luminosity should relate to $B_{\rm gq}$. We assumed that $B_{\rm gq} = c \log \rho$ and calibrated this relation using the gas densities from X-ray observations of 21 Abell clusters by Jones & Forman (1984) for which Yee & López-Cruz (1999) have calculated $B_{\rm cg}$. The median density and cluster richness for these 21 clusters was found to be $3.03 \times 10^{-3}\,{\rm cm}^{-3}$ and 1075 Mpc$^{1.77}$. We took this combination of ρ and $B_{\rm cg}$ to be typical for rich clusters. For galaxies with no enhancement in the surrounding galaxy density, we used $B_{\rm gg} =$ 60 Mpc$^{1.77}$ (Davis & Peebles 1983) and a density of $3.4 \times 10^{-5}\,{\rm cm}^{-3}$, which is a typical gas density at 100 kpc in isolated ellipticals (Forman, Jones & Tucker 1985). This gave a slope of $c = 520.6$ for the $B_{\rm gq}$–$\log \rho$ relation.

We then assumed that $L_{408\,{\rm MHz}} \propto r^{\alpha} \rho^{7/12}$, as predicted by simple analytical models of radio sources (e.g. Miller, Rawlings & Saunders 1993). The slope, α, was found by fitting a straight line to the data in a $\log L_{408\,{\rm MHz}}$–$\log r$ plot, which came out as $\alpha = -0.408$. For consistency, we also found the best-fitting slope for the extended (>30 kpc) sources only, which gave $\alpha = -0.239$. It is interesting to note that the quasars show an anticorrelation between radio luminosity and size, but that the population of radio sources as a whole does not. A likely explanation could be the optical selection effects in the 7C sample. Also the emission at lower frequencies might be absorbed in the CSS sources, which would explain why there are fewer CSS sources among the 7C quasars (selected at 151 MHz) as opposed to the MRC quasars (selected at 408 MHz). The correlation between radio luminosity and size also weakens when we exclude the CSS sources.

By assuming a fixed jet power, Q, for all the sources, we then evaluated the relationship between $L_{408\,{\rm MHz}}$ and $B_{\rm gq}$ as

$$B_{\rm gq}/c = \frac{12}{7}(\log L_{408\,{\rm MHz}} - \alpha \log r),$$

in the two cases of α. The relation is plotted in Fig. 9, where the predicted slope of 12/7 is seen to be steeper than what the data indicates. So the correlation of $B_{\rm gq}$ with environment is weaker than we expect from simple models in which the density alone determines the radio luminosity. We can therefore rule out as strong a $B_{\rm gq}$–$L_{408\,{\rm MHz}}$ dependence as we would see if all objects had about the same jet power, and environment was entirely responsible for determining radio luminosity. Nevertheless, as the luminosity function for the radio jet power is likely to be steeply declining at high powers, it seems not unlikely that selection effects could operate to produce some correlation between $B_{\rm gq}$–$L_{408\,{\rm MHz}}$ without it being as strong as it would be in this rather extreme model in which the jet power is the same for all radio sources.

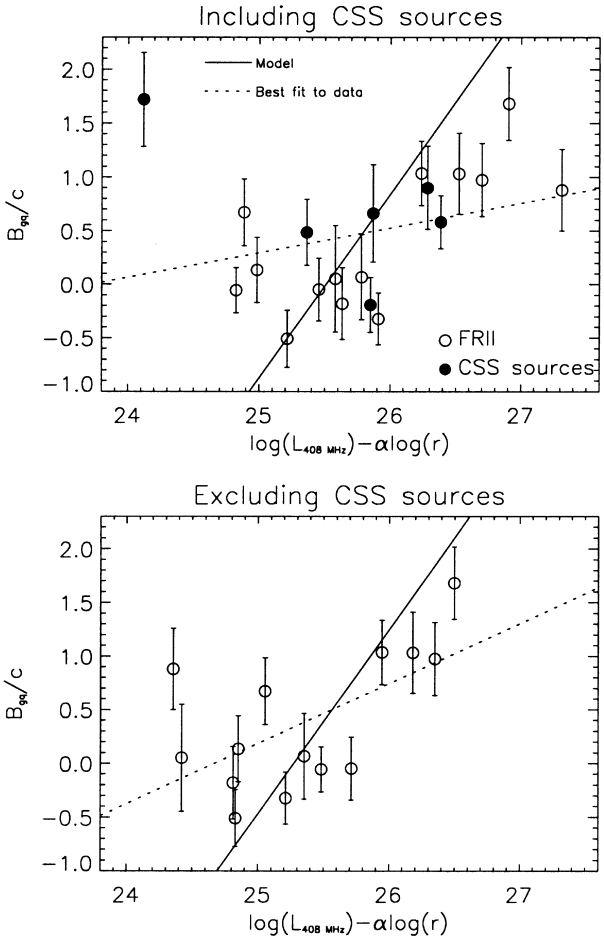

Figure 9. The solid line corresponds to the predicted relationship between quasar radio luminosity and environment from simple models assuming that environment is entirely responsible for determining the radio luminosity. The predicted correlation is much stronger than what is observed, shown by the dotted line. In this plot, we have assumed that $\log \rho = B_{\rm gq}/c$, where $c = 520.6$. The upper plot shows the relationship when all quasars are included in the fit with a radio luminosity–size slope of $\alpha = -0.408$. In the lower plot, the CSS sources in the sample have been ignored, and $\alpha = -0.239$. It may be noted that this rather simple model goes very quickly to negative $B_{\rm gq}$ values. This is implicit in the model due to the assumption that $B_{\rm gq}$ is proportional to $\log \rho$.

Given the large scatter in both the $B_{\rm gq}$–$L_{408\,{\rm MHz}}$ and the $L_{408\,{\rm MHz}}$–$M_{\rm B}$ (or $L_{[{\rm O\,III}]}$) correlations it is quite possible that both environment and radio jet power play important rôles in determining the radio luminosity. The relationship between radio sources and their environments must be complex, and the vast majority of radio sources may lie in some sort of cluster-like environment, from groups of only a few galaxies to clusters as rich as Abell class 1 or more. The weak correlation we see can probably be explained if we assume that radio sources occupy a range of environments from fairly isolated ellipticals to rich clusters, and their radio luminosities are determined both by the environment and the kinetic power in the jets.

9 SUMMARY

We have investigated the galaxy environments around 21

radio-loud, steep-spectrum quasars in the luminosity range $23.8 \leq \log(L_{408\,\mathrm{MHz}}/\mathrm{WHz}^{-1}\,\mathrm{sr}^{-1}) \leq 26.7$ and redshift range $0.5 \leq z \leq 0.82$, and find an excess of galaxies within a 0.5-Mpc radius centred on the quasar. The galaxy excess in each quasar field was quantified using the galaxy–quasar cross–correlation amplitude, B_{gq}, and an Abell-type measurement, $N_{0.5}$. Our estimates of B_{gq} is seen to fall approximately in the same range as that found for quasar environments by other investigators. We also find that $N_{0.5}$, although originally intended for fields around radio galaxies (Hill & Lilly 1991), is applicable to quasars fields too, and that $N_{0.5}$ for our quasar fields is consistent with $N_{0.5}$ for fields around radio galaxies studied by Hill & Lilly (1991).

The average B_{gq} of our quasar sample was found to be $265 \pm 74\,\mathrm{Mpc}^{1.77}$, or in terms of r_0, the correlation length of the galaxy–quasar cross-correlation function, $r_0 = 23.4\,\mathrm{Mpc}$. If the galaxies around the quasars were distributed as low-redshift field galaxies, B_{gq} would be $\approx 60\,\mathrm{Mpc}^{1.77}$ and $r_0 \approx 10\,\mathrm{Mpc}$ as found for the galaxy–galaxy correlation function in the field (e.g. Davis & Peebles 1983). This shows that the quasars are sited in richer than average galaxy environments, and two of the quasar fields have B_{gq} above $740\,\mathrm{Mpc}^{1.77}$, considered here to be characteristic for clusters with Abell richness class 1 or greater.

Our sample extends previous quasar samples to higher redshifts whilst maintaining the same range in radio luminosity. We compared with B_{gq} measurements in fields around radio-loud quasars from these samples (YG87; EYG91; Yee & Ellingson 1993), and detected a weak, but significant, correlation between radio luminosity and environment richness. The correlation between B_{gq} and environment was found to be much weaker than expected from simple models in which gas density alone determines the radio luminosity. Probably, the correlations between B_{gq} and environment, and between jet power, Q, and quasar UV/optical luminosity can be explained if both Q and environment play significant roles in determining the luminosity of a radio source.

Studies of radio galaxies (e.g. Hill & Lilly 1991) have found that environmental richness increases with redshift and that there is no correlation with radio luminosity, contrary to our observations of radio-loud quasars. The apparent difference between radio-loud quasars and galaxies would cause problems for the unified scheme of radio-loud AGN unless the difference can be explained by selection effects or a mix of two different types of objects (Laing et al. 1994) in radio galaxy samples.

Our main conclusion is that the radio-loud steep-spectrum quasars in our sample on average occupy environments typical of poor clusters with Abell richness class 0, but that quasar environments may cover a wide range in richness, from groups of galaxies and poor clusters to clusters as rich as Abell class 1 or more. In a conventional dark matter cosmology, very rich clusters at redshifts 0.5–0.8 should be rare as they would not have had time to form. Nevertheless, a few very luminous $z \sim 0.8$–1.3 X-ray selected clusters have been found (e.g. Henry et al. 1997; Rosati et al. 1999), so at least some very gas-rich environments exist at high redshift. It is thus perhaps surprising that so few radio-loud objects are found in clusters of Abell richness 1 or higher, given the arguments about both galaxy–black hole mass and the relationship between gas density and radio luminosity. This adds weight to the suggestion that fuelling problems may be the reason why radio sources seem to prefer only moderately rich environments.

ACKNOWLEDGMENTS

We are grateful to the staff at the NOT and the McDonald Observatory for their help with the observations and to D. Burstein for kindly providing maps of galactic extinction in electronic form. We also thank S. Rawlings for communicating redshifts for the 7CQ survey prior to publication, K. Blundell for the sizes of two of the MRC quasars, and the referee, P. Hall, for helpful comments and suggestions.

ML and MW were guest observers at the McDonald Observatory. The Nordic Optical Telescope is operated on the island of La Palma jointly by Denmark, Finland, Iceland, Norway, and Sweden, in the Spanish Observatorio del Roque de los Muchachos of the Instituto de Astrofisica de Canarias. We thank the British Research Council and the Research Council of Norway for a joint travel grant, and MW acknowledges further travel support from the Research Council of Norway.

This research is partially based on observations made with the NASA/ESA *Hubble Space Telescope*, obtained at the Space Telescope Science Institute. STScI is operated by the Association of Universities for Research in Astronomy, Inc. under NASA contract NAS 5-26555. IRAF is distributed by the National Optical Astronomy Observatories, which are operated by the Association of Universities for Research in Astronomy, Inc., under cooperative agreement with the National Science Foundation. This research has also made use of the NASA/IPAC extragalactic database (NED) which is operated by the Jet Propulsion Laboratory, California Institute of Technology, under contract with the National Aeronautics and Space Administration.

REFERENCES

Abell A. O., 1958, ApJS, 3, 211
Allington-Smith J. R., Ellis R. S., Zirbel E. L., Oemler A.,Jr 1993, ApJ, 404, 521
Andersen V., Owen F. N., 1994, AJ, 108, 361
Antonucci R., 1993, ARA&A, 31, 473
Barthel P. D., 1989, ApJ, 336, 606
Barthel P. D., Arnaud K. A., 1996, MNRAS, 283, L45
Benítez N., Martínez-González E., Martín-Mirones J. M., 1997, A&A, 321, L1
Best P. N., Röttgering H. J. A., Lehnert M. D., 1999, MNRAS, 310, 223
Biretta J. A. et al., 1996, WFPC2 Instrument Handbook, Version 4.0. STScI, Baltimore,
Burstein D., Heiles C., 1982, AJ, 87, 1165
Cardelli J. A., Clayton G. C., Mathis J. S., 1989, ApJ, 345, 245
Carlberg R. G. et al., 1998, Phil. Trans. Roy. Soc. Lond. A, 357, 167
Christian C. A., Adams M., Barnes J. V., Butcher H., Hayes D. S., Mould J. R., Siegel M., 1985, PASP, 97, 363
Condon J. J., Cotton W. D., Greisen E. W., Yin Q. F., Perley R. A., Taylor G. B., Broderick J. J., 1998, AJ, 115, 1693
Croft R. A. C., Dalton G. B., Efstathiou G., Sutherland W., Maddox S. J., 1997, MNRAS, 291, 305
Croft R. A. C., Dalton G. B., Efstathiou G., 1999, MNRAS, 305, 547
Croom S. M., Shanks T., Boyle B. J., Smith R. J., Miller L., Loaring N. S., 1999, in Banday T. et al., eds, Evolution of large-scale structure – from recombination to Garching, in press
Davis M., Peebles P. J. E., 1983, ApJ, 267, 465
De Robertis M. M., Yee H. K. C., Hayhoe K., 1998, ApJ, 496, 93
Dickinson M., 1994, in Hippelein H. et al., eds, Galaxies in the Young Universe. Springer-Verlag, Berlin, p. 144
Dopita M. A., Sutherland R. S., 1995, ApJ, 455, 468
Downes A. J. B., Peacock J. A., Savage A., Carrie D. R., 1986, MNRAS, 218, 31
Eales S. A., 1985, MNRAS, 217, 149
Ellingson E., Yee H. K. C., Green R. F., 1991, ApJ, 371, 49 (EYG91)
Ellingson E., Green R. F., Yee H. K. C., 1991, ApJ, 378, 476

Fanti R., Fanti C., Schilizzi R. T., Spencer R. E., Nan Rendong Parma P., van Breugel W. J. M., Venturi T., 1990, A&A, 231, 333
Fisher K. B., Bahcall J. N., Kirhakos S., 1996, ApJ, 468, 469
Forman W., Jones C., Tucker W., 1985, ApJ, 293, 102
Fort B., Mellier Y., Dantel-Fort M., Bonnet H., Knieb J.-P., 1996, A&A, 310, 705
Fukugita M., Shimasaku K., Ichikawa T., 1995, PASP, 107, 945
Groth E. J., Peebles P. J. E., 1977, ApJ, 217, 385
Guiderdoni B., Rocca-Volmerange B., 1988, A&AS, 74, 175
Guzzo L., Strauss M. A., Fisher K. B., Giovanelli R., Haynes M. P., 1997, ApJ, 489, 37
Hall P. B., Green R. F., 1998, ApJ, 507, 558
Hammer F., Le Fèvre O., 1990, ApJ, 357, 38
Henry J. P. et al., 1997, AJ, 114, 1293
Hill G. J., Lilly S. J., 1991, ApJ, 367, 1
Hudon J. D., Lilly S. J., 1996, ApJ, 469, 519
Hutchings J. B., Gower A. C., Ryneveld S., Dewey A., 1996, AJ, 111, 2167
Jones C., Forman W., 1984, ApJ, 276, 38
Koo D. C., Ellis R. S., Windhorst R. A., 1989, in Grosbøl P., Murtagh F., Warmels R., eds, First ESO/ST-ECF Data Analysis Workshop. ESO, Garching bei München, p. 19
Kaiser C. R., Dennett-Thorpe J., Alexander P., 1997, MNRAS, 292, 723
Kapahi V. K., Athreya R. M., van Breugel B., McCarthy P. J., Subrahmanya C. R., 1998, ApJS, 118, 275
Kellerman K. I., Sramek R., Schmidt M., Shaffer D. B., Green R., 1989, AJ, 98, 1195
Kormendy J., Richstone D., 1995, ARA&A, 33, 581
Lacy M., Kaiser M. E., Hill G. J., Rawlings S., Leyshon G., 1999, MNRAS, 308, 1087
Lake G., Katz N., Moore B., 1998, ApJ, 495, 152
Large M. I., Mills B. Y., Little A. G., Crawford D. F., Sutton J. M., 1981, MNRAS, 194, 693
Laing R. A., Riley J. M., Longair M. S., 1983, MNRAS, 204, 151
Laing R. A., Jenkins C. R., Wall J. V., Unger S. W., 1994, in Bicknell G. V., Dopita M. A., Quinn P. J., eds, The First Stromlo Symposium: The Physics of Active Galaxies, ASP Conf. Ser., Vol. 54. Astron. Soc. Pac., San Francisco, p. 201
Le Fèvre O., Hudon D., Lilly S. J., Crampton D., Hammer F., Tresse L., 1996, ApJ, 461, 534
Lilje P. B., Efstathiou G., 1988, MNRAS, 231, 635
Lilly S. J., Cowie L. L., Gardner J. P., 1991, ApJ, 369, 79
Lilly S. J., Tresse L., Hammer F., Crampton D., Le Fèvre O., 1995, ApJ, 455, 108
Lin H., Yee H. K. C., Carlberg R. G., Morris S., Sawicki M., Patton D., Wirth G., Shepherd C. W., 1999, ApJ, 518, 533
Longair M. S., 1981, High Energy Astrophysics. Cambridge Univ. Press, Cambridge, p. 171
Longair M. S., Seldner M., 1979, MNRAS, 189, 433
Loveday J., Peterson B. A., Efstathiou G., Maddox S. J., 1992, ApJ, 390, 338
Loveday J., Maddox S. J., Efstathiou G., Peterson B. A., 1995, ApJ, 442, 457
Macklin J. T., 1982, MNRAS, 199, 1119
Magliocchetti M., Maddox S. J., Lahav O., Wall J. V., 1998, MNRAS, 300, 257
Magorrian J. et al., 1998, ApJ, 115, 2285
Metcalfe N., Shanks T., Fong R., Jones L. R., 1991, MNRAS, 249, 498
Miller P., Rawlings S., Saunders R., 1993, MNRAS, 263, 425
Morganti R., Killeen N. E. B., Tadhunter C. N., 1993, MNRAS, 263, 1023
Netzer H. et al., 1996, MNRAS, 279, 429
Oke J. B., 1972, ApJS, 27, 21
Peacock J. A., Nicholson D., 1991, MNRAS, 253, 307
Prestage R. M., Peacock J. A., 1988, MNRAS, 230, 131
Prestage R. M., Peacock J. A., 1989, MNRAS, 236, 959
Rawlings S., Saunders R., 1991, Nat, 349, 138
Reid A., Shone D. L., Akujor C. E., Browne I. W. A., Murphy D. W., Pedelty J., Rudnick L., Walsh D., 1995, A&AS, 110, 213
Riley J. M., Rawlings S., McMahon R. G., Blundell K. M., Miller P., Lacy M., Waldram E. M., 1999, MNRAS, 307, 293
Rocca-Volmerange B., Guiderdoni B., 1988, A&AS, 75, 93
Roche N., Eales S., Rawlings S., 1998, MNRAS, 297, 405
Rosati P., Stanford S. A., Eisenhardt P. R., Elston R., Spinrad H., Stern D., Dey A., 1999, AJ, 118, 76
Rossitter D. A., 1987, PhD thesis, Univ. Cambridge
Schechter P., 1976, ApJ, 203, 297
Scheuer P. A. G., 1987, in Zensus J. A., Pearson T. J., eds, Superluminal Radio Sources. Cambridge Univ. Press, Cambridge, p. 104
Schmidtke P. C., Windhorst R. A., Mutz S. B., Pascarelle S. M., Franklin B. E., Griffiths R. E., 1997, AJ, 113, 569
Schneider P., van Waerbeke L., Mellier Y., Jain B., Seitz S., Fort B., 1998, A&A, 333, 767
Seldner M., Peebles P. J. E., 1978, ApJ, 225, 7
Serjeant S. B. G., 1996, DPhil Thesis, Univ. Oxford
Serjeant S., Rawlings S., Lacy M., 1997, in Clements D. L., Perez-Fournon I., eds, Quasar Hosts Conference. Springer-Verlag, Berlin, p. 188
Serjeant S., Rawlings S., Maddox S. J., Baker J. C., Clements D., Lacy M., Lilje P. B., 1998, MNRAS, 294, 494
Smail I., Hogg D. W., Yan L., Cohen J. G., 1995, ApJ, 449, L105
Small T. A., Ma C. P., Sargent W. L. W., Hamilton D., 1999, ApJ, 524, 31
Smith E. P., Heckman T. M., 1990, ApJ, 348, 38
Smith E. P., O'Dea C. P., Baum S. A., 1995, ApJ, 441, 113
Steidel C. C., Hamilton D., 1993, AJ, 105, 2017
Stockton A., 1978, ApJ, 223, 747
Taylor G. L., Dunlop J. S., Hughes D. H., Robson E. I., 1996, MNRAS, 283, 930
Valdes F., 1989, in Grosbøl P. J., Murtagh F., Warmels R. H., eds, Proceedings of the 1st ESO/ST-ECF Data analysis Workshop. ESO, Garching bei Múnchen, p. 35
Wilkinson P. N., Akujor C. E., Cornwell T. J., Saika D. J., 1990, MNRAS, 248, 86
Willott C. J., Rawlings S., Blundell K. M., Lacy M., 1998, MNRAS, 300, 625
Willott C. J., Rawlings S., Blundell K. M., Lacy M., 1999, MNRAS, 309, 1017
Wurtz R., Stocke J. T., Ellingson E., Yee H. K. C., 1997, ApJ, 480, 547
Yates M. G., Miller L., Peacock J. A., 1989, MNRAS, 240, 129
Yee H. K. C., Ellingson E., 1993, ApJ, 411, 43
Yee H. K. C., Green R. F., 1984, ApJ, 280, 79
Yee H. K. C., Green R. F., 1987, ApJ, 319, 28 (YG87)
Yee H. K. C., López-Cruz O., 1999, AJ, 117, 1985
Zirbel E. L., 1997, ApJ, 476, 489

This paper has been typeset from a TEX/LATEX file prepared by the author.